

Review

Montmorillonite for Adsorption and Catalytic Elimination of Pollutants from Wastewater: A State-of-the-Arts Review

Zakariyya Uba Zango^{1,2,*}, Abdurrahman Garba¹, Zaharaddeen Nasiru Garba³, Muttaqa Uba Zango⁴, Fahad Usman² and Jun-Wei Lim^{5,6,*}

¹ Department of Chemistry, College of Natural and Applied Science, Al-Qalam University Katsina, Katsina 2137, Nigeria

² Institute of Semi-Arid Zone Studies, Al-Qalam University Katsina, Katsina 2137, Nigeria

³ Department of Chemistry, Ahmadu Bello University, Zaria, P.M.B, Kaduna 1044, Nigeria

⁴ Department of Civil Engineering, Kano University of Science and Technology, Wudil, P.M.B, Kano 3244, Nigeria

⁵ HICoE-Centre for Biofuel and Biochemical Research, Institute of Self-Sustainable Building, Department of Fundamental and Applied Sciences, Universiti Teknologi PETRONAS, Seri Iskandar 32610, Perak Darul Ridzuan, Malaysia

⁶ Department of Biotechnology, Saveetha School of Engineering, Saveetha Institute of Medical and Technical Sciences, Chennai 602105, India

* Correspondence: zakariyyazango@auk.edu.ng (Z.U.Z.); junwei.lim@utp.edu.my (J.-W.L.)

Abstract: Clay minerals have been recognized as one of the cheap and effective materials for wastewater remediation. Among the various clay minerals, montmorillonite (MMT) has received much attention due to its wide availability, low-cost and promising properties such as high porosity, mechanical strength, and cation exchange capacity. Additionally, MMT has high swelling properties. These features make it an ideal material for wastewater remediation applications. In addition, it possessed good cationic exchange capacity, making it easier to interact with various molecules. MMT and its composites exhibited good selectivity and catalytic activity for contaminants elimination from wastewater. Surface modification and functionalization have been identified as a way to improve the MMT's adsorptive performance and endow it with light and light-harnessing properties. Thus, MMT composites, especially metal and metal-oxide nanoparticles, have shown good adsorption and photocatalytic activity toward the elimination/mineralization of various contaminants such as dyes, pharmaceuticals, heavy metals, and other organic and inorganic species. As such, MMT and its composites can be adopted as potential materials for wastewater remediation.

Keywords: adsorption; catalytic elimination; montmorillonite; pollutants; photocatalysis



Citation: Zango, Z.U.; Garba, A.; Garba, Z.N.; Zango, M.U.; Usman, F.; Lim, J.-W. Montmorillonite for Adsorption and Catalytic Elimination of Pollutants from Wastewater: A State-of-the-Arts Review. *Sustainability* **2022**, *14*, 16441. <https://doi.org/10.3390/su142416441>

Academic Editors: Luca Di Palma and Steve W. Lyon

Received: 10 November 2022

Accepted: 6 December 2022

Published: 8 December 2022

Publisher's Note: MDPI stays neutral with regard to jurisdictional claims in published maps and institutional affiliations.



Copyright: © 2022 by the authors. Licensee MDPI, Basel, Switzerland. This article is an open access article distributed under the terms and conditions of the Creative Commons Attribution (CC BY) license (<https://creativecommons.org/licenses/by/4.0/>).

1. Introduction

Recently, population explosion/growth and industrialization increased the demand for freshwater. It is predicted that the availability of fresh water to the general population will decrease by 2050, and the demand for it will rapidly rise, which could eventually create water scarcity. In addition to rapid industrialization, global warming due to anomalous climate change is another factor that disturbs groundwater development [1,2]. The quality of water resources is fast decreasing due to the persistent release of organic and inorganic contaminants from both natural and anthropogenic sources [3]. The discharge of many hazardous contaminants such as pharmaceuticals, dyes, pesticides, herbicides, fertilizers, nuclear wastes, heavy metals, and other waste into water bodies resulted in pollution, which affects the sustainability of living organisms [4,5]. Contamination of water is of vital concern as it has staggering effects on the environment. Its negative impact on domestic consumption, agriculture, recreation, fishing, and other industrial activities is noticeable. Although some industries are equipped with waste treatment facilities, lack of proactive measures, efficient policies, reluctance to adopt advanced technologies, as well as lack of

suitable remediation technologies often strengthen pollution generation [6]. Thus, polluted water threatens human health and the environment at large. Moreover, the presence of such pollutants in the environment, even at low concentrations, poses a major threat to both fauna and flora [7]. Upon discharge, these pollutants are transported into local reservoirs, rivers, ponds, and other sources of fresh water, which accumulate in plants and aquatic organisms and are eventually consumed by humans in foods and drinking water. Some of these pollutants are associated with high toxicity and carcinogenic and mutagenic tendencies, thus, posing a threat to the sustenance of living organisms [8].

Water pollution control is one of the main agendas for the United Nations 2030 vision toward achieving Sustainable Development Goals (SDGs), stressing the need for clean water and sanitation. Industrial treatment plants utilize biological, chemical, or physical methods to safeguard water bodies from pollutants [9]. The biological methods depend on biodegradation using microorganisms such as *Mycobacterium*, *Bacillus*, *Pseudomonas*, *Sphingomonas*, and others which were found to be ineffective for dyes [10]. On the other hand, chemical methods rely on processes such as flocculation [11], coagulation [12], electro-flocculation advanced oxidation [13], and photocatalytic degradations [14]. At the same time, physical methods depend on adsorption [15] and membrane filtration techniques [16]. However, the majority of such techniques have disadvantages that restrict their application for the decontamination of wastewater. For example, membrane separations and evaporation involve high investment and as well as high maintenance costs [17], while aerobic and anaerobic digestion processes require complex and skilled operation procedures [18]. Moreover, other techniques like flocculation and coagulation require the use of a large number of chemicals that may produce unwanted by-products, which may cause additional harmful effects to the environment. Due to the aforementioned limitations of the listed techniques, it becomes necessary to find an efficient and sustainable method for the treatment of wastewater [19]. Among these techniques, the physical methods were the most preferred, especially those based on adsorption and photocatalytic degradation [20,21].

Adsorption has been identified as an exceptionally efficient, simple, low-cost, recyclable as well as an eco-friendly technology for pollutant mitigation in environmental waters [22]. In addition, natural and synthetic adsorbents are available with high specific surface area and appropriate pore structure, and they are easily prepared [23]. The pore in the adsorbents can trap the pollutants molecules through various interactions such as van der Waals attractions in the case of physical adsorption (physisorption) or hydrogen and covalent and, in some cases, electrostatic attraction when chemical adsorption (chemisorption) is involved. The technique is considered an efficient tool for the remediation of contaminants from environmental waters as it does not lead to secondary pollution [24]. Used clay minerals [25], zeolites [26], activated carbon (AC) and carbon nanotubes (CNTs) [27], graphene and graphene oxides [28,29], metal-organic frameworks (MOFs) [30], etc., have been discovered for contaminants elimination from wastewaters. Amongst such adsorbents, clay minerals and their derivatives were identified as promising techniques for wastewater treatment due to their structural features [31]. They are composed of a large family that is distinct from other adsorbents regarding their microstructure, adsorptive properties, and environmental applications. Nowadays, this large family of adsorbents is attracting much attention for contaminants removal from polluted air, soil, and wastewater. If not all, one may proclaim that all the contaminants discovered so far have a suitable adsorbent for their removal from the environment.

On the other hand, photocatalytic degradation is an advanced oxidation process that offers a good alternative for the complete mineralization of pollutants. It involves the use of heterogenous photocatalyst with semiconducting properties that harness radiation from either natural source (sunlight) or from artificial sources (such as hollow cathode lamp) to generate the excited electrons (e^-) and holes (h^+) that attack the pollutant molecules. Thus, the primary requirements of the photocatalyst material include its ability to undergo electron excitation upon light irradiation and sufficient porosity to allow the adsorption of pollutant molecules [32]. The most dominant photocatalyst is titanium oxide (TiO_2)

due to its good semiconducting property and ability to utilize visible light [33]. It has been widely employed for the photocatalytic degradation of various organic and inorganic pollutants [34]. It allows for the transformation of the pollutants upon excitation by light and photogenerated electrons from the photocatalyst to other chemical species, which are less harmful than the original form [35]. It involves breaking down chemical bonds in the pollutant molecules through the action of activated free radicals [34]. The final products being the carbon dioxide and water. Although it is a success, TiO_2 suffered major shortcomings, including low adsorption capacity, agglomeration in an aqueous medium, and frequent recombination of photoexcited species (e^-/h^+). These necessitate its modification for the target application [36]. Apart from the TiO_2 , other active photocatalytic materials were discovered, and functionalization of existing materials have been put forward to achieve the desired results.

In the last two decades, adsorption and photocatalysis technologies have interestingly witnessed a breakthrough in their applications as an efficient method for contaminants remediation from aqueous solutions [37,38]. Thanks to material science and engineering, various materials have been discovered and explored for the execution of two applications. Naturally occurring and synthesized materials, such as biomass, clay, rock, and soil minerals, have been utilized. Moreover, researchers utilized animal remains such as bones, chitin, shells, and cartilage of fishes, crustaceans, and other organisms. Advanced materials have also been synthesized, such as metal-oxide nanoparticles, carbon quantum dots, zeolites, mesoporous silica, molecularly imprinted polymers, CNTs, and MOFs [39,40]. The major interface for the two processes is the ability of the material to effectively trap the pollutant molecules on their surface to easily attained the adsorption-desorption equilibrium.

Clays minerals have long been recognized as potential materials for wastewater remediation. They are a class of hydrated phyllosilicates that play an important role in the formation of the smooth part of rocks, sediments, and soil [41]. They are composed of tetrahedrally and octahedrally joined atoms, forming silicate sheets with tetrahedral and octahedral shapes with a thickness usually less than 2 nm [42]. The tetrahedral sheet is made of SiO_4 layers that share three oxygen atoms which form a hexagonal arrangement [43]. The other oxygen atom (fourth oxygen or apical oxygen) of each tetrahedron is vertically aligned with the basal sheet [44]. The octahedral sheets usually have cations such as Al, Mg, or Fe attached to six equidistant anions like oxygen or hydroxyl groups [45]. Clays are easily available, relatively cheap, naturally occurring, widespread, and non-toxic, making them important in pollution remediation processes [46]. The adsorption capacity of clays is usually governed by how the adsorbate ions or molecules interact with the surface of the clays in which they share one or more oxygen atoms or hydroxyl groups. They are excellent adsorbents due to their porous structure, high surface area, high cation exchange capacity, as well as the presence of Bronsted and Lewis acidity, which make them remarkable adsorbents for several ions and molecules [46,47]. Minerals such as montmorillonite (MMT) [48], halloysite [49], palygorskite [50], and kaolinite [51], with varying sizes and textures as well as different chemical compositions, were known to exist naturally in various places of the world and have been explored for environmental remediation applications.

1.1. MMT for Wastewater Remediation Applications

Among the various clays, MMT has been well-researched due to its potential features. MMT is a member of the smectite group that is formed as a layered silicate [52]. It consists of an octahedral alumina sheet sandwiched between two tetrahedral silica sheets (Figure 1). It has a permanent negative charge due to the isomorphic substitution of the tetrahedral layer by Al^{3+} in place of Si^{4+} and in the octahedral layer by Mg^{2+} in place of Al^{3+} [6]. The negative charge in its lattice structure is neutralized by the existence of exchangeable cations such as Na^+ and Ca^+ [53], which help in adsorbing cationic species from contaminants through ion exchange [53]. The charge on this group is determined by their ability to participate in ion exchange which strongly influences their adsorptive potentials. MMT possesses excellent intrinsic physical and chemical properties such as high porosity, large

specific surface area, and smooth texture [41]. Advancements in material science in relation to environmental remediation have led to the exploration of adsorption and catalytic elimination of pollutants [54]. The unique approach to further increase the surface area, hydrophobicity, and adsorptive capacity of the MMT is by immobilizing a semiconductor on its surface [53]. The presence of a weak bond between the layers of the semiconductor and the MMT provides an excellent cation exchange and photoactive property [53]. Thus, MMT has been utilized as potential material for pollutant elimination toward a greener and more sustainable water regeneration.

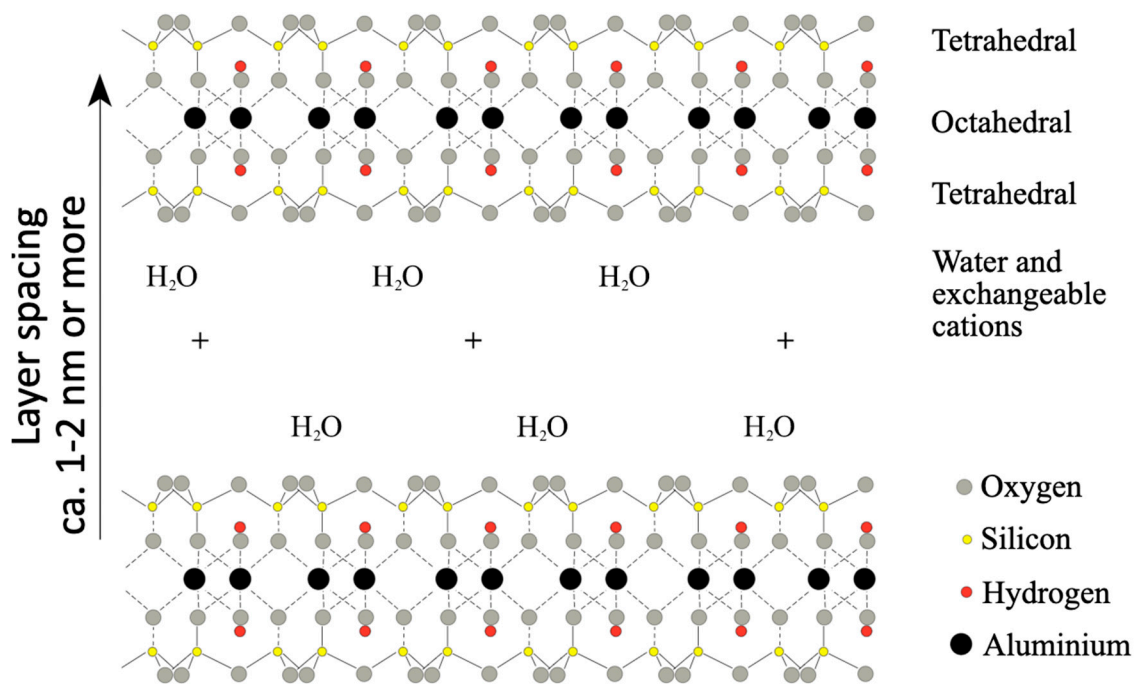


Figure 1. Structure of Montmorillonite Clay.

A glimpse into the scientific articles database has shown that a considerable number of articles have been published on the use of MMT for environmental remediation applications. ScienceDirect database specifically revealed that over 8000 articles had been written on the application of MMT for pollutants adsorption. In the year 2022 alone, 1291 have been published. While on photocatalytic elimination of pollutants, over 1700 papers have been written, of which 376 have been published in 2022. Figure 2 summarizes the number of articles reported on pollutants adsorption and photocatalytic degradation of pollutants from 2012–2022 (data obtained from ScienceDirect). Despite the massive success achieved by the MMT in the elimination of contaminants from wastewater, no comprehensive review was dedicated to discussing its recent progress in adsorption and catalytic remediation. The review presented by Wang and co-workers largely emphasized the methods for the preparation of two-dimensional MMT nanocomposites and very little was discussed on its application for wastewater remediation [6]. Thus, this article is aimed at reviewing findings presented on the application of MMT for pollutants adsorption and catalytic elimination. The potential features of MMT, modification and application for wastewater remediation have been explored, and the mechanism for the processes was highlighted.

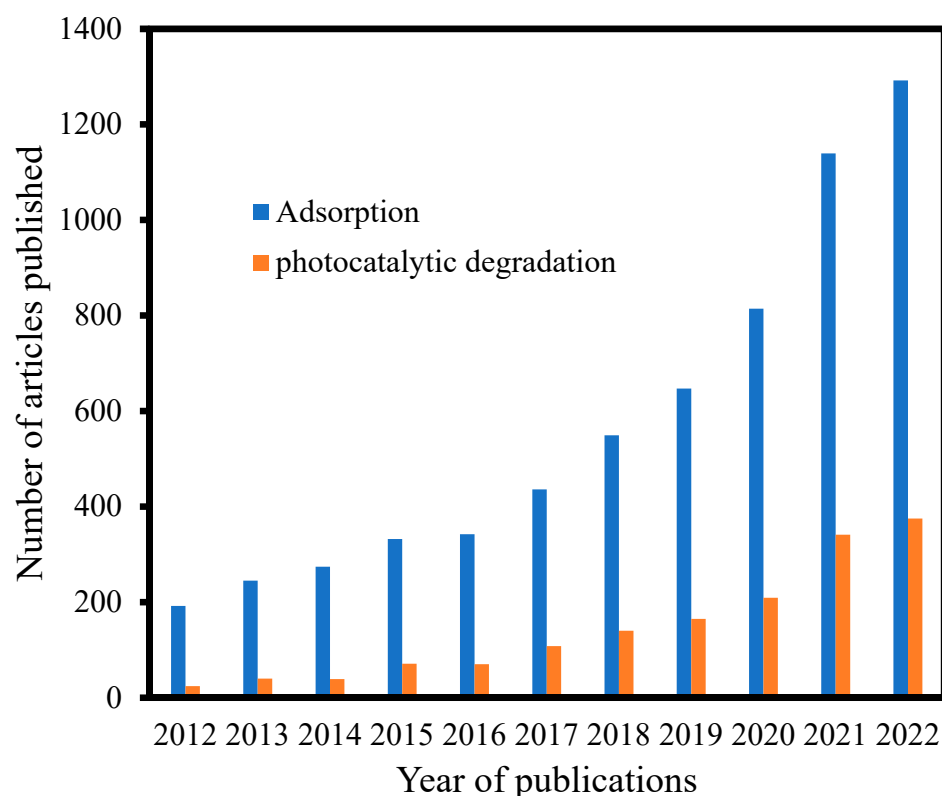


Figure 2. Number of articles published from 2012–2022 on wastewater remediation using MMT and its composites. The data is obtained from ScienceDirect (Keywords: Adsorption, photocatalytic degradation, Montmorillonite).

1.2. Modification of MMT for Wastewater Remediation

Functionalization or modification is the process of altering the materials physically or chemically so as to introduce some desired groups onto the surface of materials which will boost its capacity for a targeted application. The process also describes manipulations of surfaces using different techniques so as to tailor the surface properties to meet specific needs [2]. MMT has attracted the attention of researchers in the field of wastewater remediation not only due to its high reservation and low cost but also because of its high cationic exchange capacity resulting from its double-layered structure [55]. Despite that, its hydrophilic surface posed a threat to its dispersion in the aqueous and organic phases [56]. Thus, its functionalization/modification gives more access to the production of cheap composites with high adsorption capacities [57], light absorption and semiconducting property [58,59], biocompatibility, resistance to rough conditions [60], and ease of regeneration [61]. At the same time, these properties allow for high adsorption and photocatalytic degradation of the pollutants even amidst abundant competing ions.

1.2.1. Metal and Metal-Oxide Nanoparticles Modification

Surface modification of MMT with metal and metal oxide nanoparticles has been identified as one of the best approaches to enhance the properties of MMT. These include its crystallinity [62], mechanical strength [63], moisture, chemical and thermal stability [64], cationic exchange capacity, surface porosity [65], and photoluminescence response [66] improvements. It was also reported that the insertion of metal or metal-oxide nanoparticles into the MMT layered structure produced the MMT surface containing metal/metal-oxide with good stability [67,68]. It forms novel heterogenous structures of nano-pillars, nanorods, nanosheets, and nanowires with diversifying functionalities and semiconducting properties. Thus, various techniques for the preparation of metal-oxide/MMT composites have been explored, such as sol-gel [69], hydrothermal and modified hydrothermal growth [70,71],

precipitation, microwave [72], chemical vapor deposition [73], immobilization [74,75], dispersion [76], impregnation [77,78], and doping [79,80] techniques. Most of the techniques are eco-friendly, low-cost, and carried out at ambient atmospheric conditions.

Of the various metal-oxide nanoparticles, TiO₂ has been widely investigated. For metal-oxide modification, Hassaini et al. explored the dispersion of TiO₂ on the surface of the MMT for photocatalytic applications. SEM image of the nanocomposite revealed its heterogenous surface, indicating the distortion of the MMT layered and the successful dispersion of the TiO₂ on the MMT surface. Similarly, the N₂ adsorption–desorption result has shown an improvement in the surface porosity of the material, with the corresponding pore size of 2.62 and 3.87 nm for the MMT and TiO₂/MMT, respectively [13]. Using the dispersion technique, TiO₂/MMT formed both electrostatic and covalent bonds with the MMT by distributing itself uniformly on the MMT surface [65]. The one-step hydrothermal method for the synthesis of metal-oxide/MMT nanocomposite has also been regarded as a promising facile technique due to the formation of heterostructure nanocomposite with proper interfacial bonding. In addition to that, the synergistic effect of the MMT and the metal-oxide nanoparticle resulted in a stable nanocomposite with effective photon adsorption [71]. Based on that, He et al. reported on the growth of MnO₂ in the MMT surface via a low-temperature hydrothermal method. Fourier Transform Infrared (FTIR) spectrum of the resulting nanocomposite indicated peak disappearance at 3629 cm⁻¹ because of H₂O molecules replacement by the MnO₂, confirming the formation of MnO₂-MMT heterojunction structure [59]. Similarly, the hydrothermal technique was employed for the synthesis of MgFe₂O₄/MMT for heavy metals remediation from contaminated soil. The pore volume of the resulting composite was much higher than the MMT, indicating its good application for the intended study [81]. TiO₂-doped MMT has shown wider ultraviolet light absorption properties toward alleviation of asphalt bitumen aging and degradation of automobile exhaust [82].

On the other hand, the incorporation of the metal nanoparticles into the interlayered MMT cavities is also adopted as an effective approach to enhance the performance of the material for various applications. It has been well-reported to improve the porosity of the clay for the adsorption of molecules. The MMT layered structure often prevents the beam of light from penetrating for photo-response-related applications. However, enriching the MMT surface with metal nanoparticles such as Fe (III) resolved the issue by destroying the MMT's octahedral structure [60,63]. In addition to that, upon light irradiation, the metal nanoparticles could produce exciting photogenerated electrons, which can attack pollutant molecules in photocatalytic studies [83]. Sirajudheen and Meenaksh reported on the incorporation of Lanthanum (III) (La³⁺) into CS-MMT composite by precipitation method [84]. The result from Scanning Electron Microscopy (SEM) analysis has shown the interconnection of La³⁺ with the CS-MMT surface formed a flexible lamellar interconnected structure with a rough surface for good adsorption of guest molecules [84]. Xiang et al. also reported on the sol-gel method for the doping of Bismuth (Bi³⁺) into the surface of TiO₂/MMT nanocomposite. X-ray Diffraction (XRD) studies have demonstrated a shift in peak at 2θ equal to a 25.5 shift to a low angle. In addition to that, the peak intensity due to TiO₂ decreased, confirming the successful doping of the Bi³⁺ onto the TiO₂/MMT surface [85]. A wet impregnation technique was also employed for the synthesis of Ag-Bi₂O₃/MMT. The presence of Ag on the surface of the material improved its surface area and facilitated its utilization of visible light by lowering its bandgap [86]. Gonzalez et al. also synthesized Ti-doped MMT with enhanced photochemical properties. The composite material has shown a remarkable response to UV light illumination. In addition to that, its good crystallinity and porosity have been emphasized for trimethoprim degradation [79].

1.2.2. Surfactant Modifications

Surfactants have grown in popularity for MMT modifications. They are referred to as surface-active substances that can potentially change the surface behavior of materials for a particular application [87]. Natural MMT has a layered structure, high hydrophilicity,

and characteristics resembling those of colloids [88,89]. Positively charged cations can be adsorbed on the surface of MMT by ion exchange, van der Waals force, and functional groups that contain oxygen [90].

The strong hydrophilicity and small interlayer spacing of natural MMT resulted in its limited adsorption capacity for organic pollutants adsorption and catalytic elimination [56]. Therefore, to boost the ability of MMT to adsorb organic pollutants, it must be modified to create organo-MMT with hydrophobic surfaces [91]. The most used surfactants as modifiers for the MMT are the single-chain surfactants such as cetyltrimethylammonium ammonium bromide (CTAB), trimethylphenyl ammonium (TMPA), benzyl triethylammonium (BTEA), and tetramethylammonium (TMA) [56,92]. However, the above cationic surfactants show certain aquatic toxicity, which limits the application of modified MMT. In order to reduce their toxicity, some studies introduced the ester group on the cationic surfactant, such as the substitute of dioctadecyl dimethyl ammonium chloride cationic ester-containing Gemini surfactant, which is a new type of non-toxic and biodegradable cationic surfactant has been explored. These include long-chain surfactants such as 1,3-bis(dodecyltrimethylammonium) propane dibromide (BDP), 1,3-bis(dodecyltrimethylammonium)-2-hydroxypropane dichloride (BDHP), didodecyldimethylammonium (DDDMA), cetyltrimethylammonium (CTMA), and hexadecyltrimethylammonium (HDTMA) [93,94]. This is due to their thermal stability and amazing chemical structure, which make them convert their hydrophilic surfaces to hydrophobic ones for the uptake of organic contaminants [95]. The improved adsorption capacities of the modified organo-MMT were not only due to the acquired hydrophobic surfaces but were also due to the swelling of the MMT's interlayer spacing [96].

The use of gemini surfactants has been widely reported for the removal of hydrophobic compounds from wastewater. Gemini surfactants comprise of aromatic ring attached to an alkyl chain which enables the modified MMT to have the advantage of having a hydrophobic surface with a special π - π interaction with the pollutants. Gemini surfactant intercalated clays demonstrated high removal capacity for bisphenol A [92], triclosan [56], pharmaceutical drugs [97], and many other organic and inorganic pollutants. The remediation of pollutants by MMT has been based on physical or surface adsorption that was driven by van der Waals forces, or it was based on partitioning across phases that depend on the surfactant length [92,98]. Hongling et al. reported the adsorption of two β -blocker pollutants (Atenolol and acebutolol) on a hexadecanoamide propyl trimethylammonium chloride modified MMT, which is a common quaternary alkylammonium salt. They pointed out that the adsorption capacity of the modified MMT doubled compared to the natural form and suggested that both electrostatic interaction (π - π interaction) and the hydrophobic partitioning between the organo-MMT and the two pollutants may be responsible for the increased adsorption of the pollutants [97]. Zhongxin et al. reported that modification of MMT with hexamethylene bispyridinium dibromides (HMBP) shows the highest adsorption capacity for phenol among phenolic derivatives. This was credited to the π - π interaction between pyridine and benzene rings in the phenols. Hence, the affinity for a certain pollutant molecule depends on the chemical structure of the surfactant [99]. Therefore, to enhance the removal of a target pollutant molecule, a surfactant with a special function group must be employed.

1.2.3. Polymer Modification

Researchers have also carried out MMT modification using polymers with the aim of obtaining the benefits of the two materials combined in one single form and overcoming their individual limitations. For example, MMT has lower recovery in aqueous solutions, which limits the potential for micro-pollutants remediation [100]. On the other hand, polymeric resins have shown promising potential to overcome clay's limitations, but their properties, such as high cost, pH dependence, particle size sensitivity, and poor water wettability, hinder their use for industrial and water treatment applications [46]. Moreover, MMT is hydrophilic and can mix with hydrophilic polymers in all ratios, such as

poly(vinyl alcohol) [101] and poly (ethylene oxide) [102] and many others. Therefore, for MMT to be compatible with hydrophobic polymers, their hydrophilic surface must be made hydrophobic through conversion to organoclays. Hence, various techniques for the preparation of polymer/MMT composites have been explored, such as melt intercalation [103], blending [53], polymerization [104], wet impregnation [93], non-solvent induced separation [105], hydrothermal process [105], co-precipitation [106], and grafting [94]. Most of the methods applied for the synthesis of these composites were low-cost, eco-friendly, and as well conducted at moderate reaction conditions.

For MMT modification with organic polymers, Salah et al. reported the synthesis of chitosan/MMT composite for the removal of methylene blue in aqueous media. The composite formation was confirmed using SEM, XRD, FTIR, pH_{pzc} , XPS, TGA, and water regain analysis. The novel composite displayed multilayer heterogenic physical adsorption for Dubinin–Radushkevich and Freundlich adsorption isotherms and fitted well with the pseudo-second-order kinetics better than pseudo-first-order kinetics, indicating that both the MB and the composite played a part in the adsorption process. Moreover, the novel composite demonstrated a good desorption ratio of 97% even during the first regeneration cycle [107]. Moreover, Zhang et al. reported the synthesis, characterization, and subsequent adsorption of Eosin Y on MMT/polypyrrole nanocomposite that was prepared via in situ polymerization of pyrrole monomer on MMT. The maximum adsorption capacity of 112.5 mg/g at 35 °C for the nanocomposite was reached after 20 min. The adsorption kinetics proved that there was a rapid uptake of the pollutant by the composite, and the pseudo-second-order model well fitted the adsorption. Likewise, the isotherm data for the experiment agree with the Langmuir model and the adsorption thermodynamic analysis showed that the adsorption process was spontaneous and endothermic [108]. Moreover, Amaly et al. synthesized a microcrystalline cellulose/MMT porous and electrostatic attracting composite aerogel for preconcentration of anions in dairy wastewater. The composite exhibited excellent adsorption capacity for nitrate ions. The composite was characterized by high mechanical strength, and fast recovery of 80% at faster flow rates. Most importantly, the composite can preconcentrate low nitrate concentrations in dairy wastewater in comparison to commercially prepared resins [109].

2. MMT for Pollutants Adsorption

2.1. MMTs for Dyes Adsorption

Dye-related water contamination has long been recognized as a serious environmental problem. There is a wide variety of dyes with various chemical structures in the wastewater from the textile, plastics, leather, petrochemical, and related industries. Due to their numerous industrial applications, dyes that are considered toxic chemicals are being used at an alarmingly increased rate [110]. They are employed extensively in a variety of industrial processes, including those that produce paper and pulp, plastics, dye clothing, treat leather, and print, which later cause soil and water contamination because of the presence of industrial effluents containing dyes [111]. Due to their toxicity and the fact that most of them are resistant to microbial degradation, the presence of these dyes in the environment is undesirable. Due to their capacity to undergo anaerobic degradation, some dyes also cause the formation of chemicals that may be carcinogenic [112]. Another danger posed by dyes in the environment is that the highly colored wastewater they produce may prevent sunlight and oxygen from reaching different aquatic creatures, which could result in their extinction. Therefore, it is crucial to keep an eye on and manage how these colors enter water systems. Adsorption is the most extensively used method for removing dyes and other impurities from contaminated water because it is efficient at removing a high proportion of colors over a wide concentration range [113]. Due to its low cost, simplicity of use, and seemingly limitless supply of adsorbents from both natural and synthetic sources, the adsorption method has received attention in much of the literature. Table 1 highlights the proven efficacy of clay minerals in the adsorption of contaminants and their potential to filter out both organic and inorganic species from environmental waters.

A cost-effective and environmentally friendly nanocomposite CH-Mt/PANI was synthesized as an adsorbent by Minisy and co-workers using CH, a natural biodegradable polymer, Mt, a clay mineral with high cation-exchange capacity, and conducting PANI with good chemical and environmental stability [114]. Methylene blue (MB), a cationic dye used as a model organic pollutant, was then adsorbed from aqueous solutions using the nanocomposite. Temkin isotherm model well described the pseudo-second-order kinetics of the dye adsorption onto the CH-Mt/PANI base nanocomposite. Additionally, it was discovered that intraparticle diffusion was crucial to the adsorption mechanism. According to estimates, the highest adsorption capacity was 111 mg/g, which was more than the combined adsorption capacities of the precursors [114]. Recently, Yilmazoglu et al. created two distinct imidazole-based ionic liquids (ILs), N-methylimidazolium tetrafluoroborate (MIM) and N-butylimidazolium tetrafluoroborate (BIM), with various alkyl chain lengths and used them to modify montmorillonite (MMT). They conducted a thorough analysis of the IL-modified MMT clays' capacity to adsorb Orange II (O-II) anionic dye and remove it from aqueous solutions. The maximum adsorption capacities were achieved at pH 2. For MMT, MIM-MMT, and BIM-MMT, the adsorption capacities were determined to be 1.26 mg/g (75%), 2.29 mg/g (90%), and 1.70 mg/g (84%), respectively. The experimental isotherm data and the Freundlich model agreed well, indicating that the adsorption of the O-II dye took place on the heterogeneous surface sites of the adsorbent. Additionally, a pseudo-second-order kinetic model demonstrated that the primary mechanism for the adsorption process was physisorption. Their findings showed that the addition of ILs to MMT enhanced the clay's ability to adsorb O-II from aqueous solutions. It was also discovered that MIM-MMT samples with short alkyl chains can serve as an alternative to clay and function as efficient adsorbents for the removal of harmful O-II dye pollutants and for further comprehension of the dye adsorption mechanisms [115].

Zhao et al. synthesized a self-assembling gel of Fe-chitosan/montmorillonite nanosheets (Fe-CS/MMTNS) for the removal of methylene blue (MB) under visible light and in the presence of H₂O₂. Through the synergistic effect of adsorption and the photo-Fenton reaction, they showed that the Fe-CS/MMTNS gel performed effectively in the removal of MB. Additionally, their gel performed well in a variety of pH situations. Because the adsorption sites of the Fe-CS/MMTNS were continuously reactivated through photo-Fenton degradation, the composite gel also demonstrated effective reusability [116]. The proposed mechanism shows that MB was degraded in two ways on Fe-CS/MMTNS in the presence of H₂O₂ under visible light irradiation (Figure 3). The first involved MB being directly exposed to photo-Fenton degradation and being oxidized into inorganics in an aqueous medium. The second involved MB being adsorbed by Fe-CS/MMTNS and being oxidized after that. In other words, MB was eliminated using a combination of photo-Fenton and adsorption. Since Cl was quickly ionized and removed from the chromophore in Figure 3, MB initially had a positive charge and an atomic weight of 284 g/mol. The other part of the MB was first adsorbed by Fe-CS/MMTNS gel, and S was oxidized into S=O, followed by its desorption, which was then captured and degraded by the reactive radicals once more. The reactive radicals then directly attacked part of the MB and gradually converted it into inorganic substances like NO₃⁻, SO₂²⁻, and CO₂ [116]. Table 1 summarizes various reports on the adsorption of dyes onto MMT and its composites. The major findings have been highlighted.

Table 1. Compilation of various MMT and composites for dye adsorption.

Adsorbent	Pollutant	Adsorption Parameters				Highlights	Ref
		pH	Temp (K)	Adsorbate Conc (mg/L)	Contact Time		
Ca-MMT Ti-MMT	BG5 BV10	-	298	-	0–250 min	<ul style="list-style-type: none"> - The smaller adsorption capacity of Ti-MMT shows that Ti^{4+} is more difficult to displace by ion exchange than Ca^{2+}. Thus, Ti-MMT possessed higher adsorption efficiency. - The process was best described as pseudo-second order. 	[117]
KG-g- PMETAC/MMT	MB TB CV	4–10	298–318	10–100	0–400 min	<ul style="list-style-type: none"> - The reusability studies indicated that desorption of about 70% of the adsorbed dyes can be achieved after two consecutive cycles. - The process follows pseudo-first-order and Freundlich kinetic and isotherm models, respectively. 	[40]
γ -Fe ₂ O ₃ @MMT	RhB	2–10	298	50–150	0–140 min	<ul style="list-style-type: none"> - Results from dynamics simulations of the adsorption of RhB dye molecules onto γ-Fe₂O₃@MMT composite assumed that RhB molecules are much more tightly bound to the MMT surface compared to the iron oxide cylindrical nanoparticle. - The process follows pseudo-second-order and Langmuir models based on the kinetic and isotherms studies. 	[118]
MMT-Li MMT-Na MMT-K MMT-Rb MMT-Cs	BMIMCl	-	-	0.5–2.7	5–75 min	<ul style="list-style-type: none"> - IL improved dye adsorption a little bit. The interaction between the dye and the IL is highlighted based on the fluorescence lifetime. This interesting result confirms that the dye is not released compared to the pristine MMT. - Pseudo-second-order and Langmuir models best described the kinetic and isotherms studies. 	[119]
Surfactant- modified MMT	CPCM ADBAC RR120	7	301	0.1–10	24 h	<ul style="list-style-type: none"> - The modified MMT exhibited higher adsorption efficiency, and the Langmuir fitting implies a chemisorption process 	[120]

Table 1. Cont.

Adsorbent	Pollutant	Adsorption Parameters				Highlights	Ref
		pH	Temp (K)	Adsorbate Conc (mg/L)	Contact Time		
MMT@NiFe LDH	MB MO	-	298	10–180	2 0–120 min	<ul style="list-style-type: none"> - Two-dimensional to two-dimensional growth of NiFe LDH nanoflakes on MMT was desirable for the removal efficiency of MO and MB dyes. - The adsorption is favored by pseudo-second-order and Langmuir models 	[121]
MMT TiO ₂ -pillared MMT	SR3BL	2.5–11	-	0–100	60 min	<ul style="list-style-type: none"> - Calcination of the MMT improved its porosity, while the TiO₂ modification improved its adsorption capacity by making the surface hydrophilic - It formed monolayer adsorption fitted by Langmuir model 	[36]
MMT-HAD	TZ	2–11	298–318	20–60	5–45 min	<ul style="list-style-type: none"> - HDA modification remarkably improved the adsorption ability of MMT toward TZ. The highest adsorption efficiency was achieved >98% at the pH range of 4–6 within a fast process (less than 30 min) - Presided by pseudo-second-order and Langmuir models 	[91]
CA/OMMT	AGB DP3B	2–9	303–323	100	0–600 min	<ul style="list-style-type: none"> - CA/OMMT nanocomposites exhibited high adsorption capacities toward AGB, which contains more than one sulfonate group. 	[122]
γ -Fe ₂ O ₃ /MMT	RhB	-	RT	10–50	0–90 min	<ul style="list-style-type: none"> - The presence of Fe₂O₃ improved the adsorption efficiency of the MMT and allowed for easy regeneration of the adsorbent. - The data were favored by the Freundlich model. 	[76]

Table 1. Cont.

Adsorbent	Pollutant	Adsorption Parameters				Highlights	Ref
		pH	Temp (K)	Adsorbate Conc (mg/L)	Contact Time		
MMT sPEEK-MMT	IB	12.5	RT	10–600	2–180 min	<ul style="list-style-type: none"> - The sPEEK interacts with the MMT via hydrogen and electrostatic interaction. The composite swells, enabling mass transfer of the IB to its surface. - The adsorption is favored by pseudo-second-order and Freundlich models. 	[123]
MMT-SDS	BR13	6	297–298	30–1000	0–120 min	<ul style="list-style-type: none"> - The modification improved the performance of the MMT and eased its regeneration. - It follows pseudo-second-order and Langmuir models. 	[61]
Chitosan/KSF-MMT	RB	2–8	RT	100–1600	0–600 min	<ul style="list-style-type: none"> - The biocomposite has shown improved properties and adsorption capacity than the pristine MMT, attributed to the crosslinking. - It follows pseudo-second-order and Langmuir models. 	[124]
PMAL-CTS/MMT	AY17 BG	2–10	298	50–70	0–300 min	<ul style="list-style-type: none"> - PMAL-CTS/MMT nanocomposite has exhibited higher adsorption efficiency toward the dyes in the single and binary systems, attributed to functional groups on its surface 	[94]
Chitosan-MMT	MB	2–8	288–308	65–400	0–8 min	<ul style="list-style-type: none"> - The composite has shown fast adsorption of the dye, attributed to the crosslinking between chitosan and MMT. - Adsorption data is well-fitting to Freundlich isotherm and pseudo-second-order kinetics. 	[107]

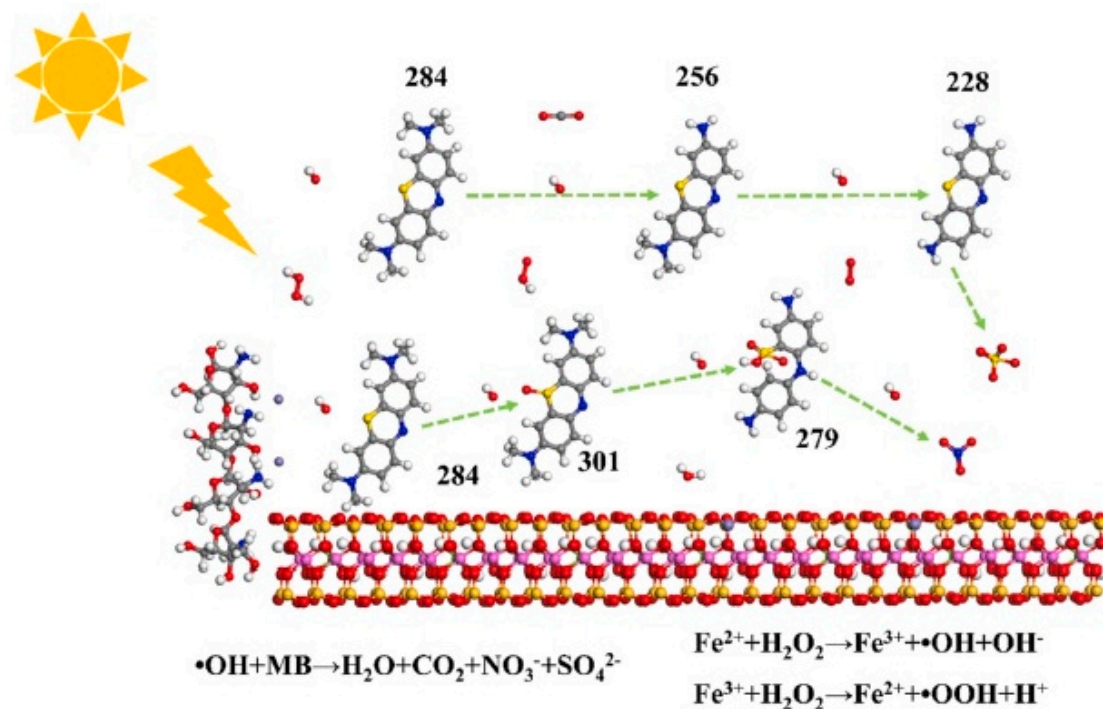


Figure 3. Schematic diagram of MB degradation on Fe-CS/MMTNS. Reproduced with permission from Reference [116].

2.2. MMTs for Pharmaceuticals Adsorption

Environmental pollution has long been linked to the discharge of pharmaceuticals, personal care items, phenols, and organic acids into environmental waters. Typically, petrochemicals, cosmetics, pharmaceuticals, and allied industries, as well as hospital discharges, are the main sources of these pollutants. Pharmaceuticals like antibiotics, antifungals, analgesics, and other medicines are made specifically to treat illnesses, but when their metabolites are found in water bodies, they are considered to be harmful [70]. The majority of the time, they enter the water through excretions and hospital discharges. Municipal wastewater contains most pharmaceuticals that have been reported to be harmful to living things. Due to these chemicals' great resistance to biodegradation, conventional wastewater treatment typically cannot eliminate them. Additionally, several pharmaceuticals have been found in seawater. They are found in these environments because contaminated wastewater effluents are carried by rivers into bigger bodies of water like oceans and seas, indicating that they can be quite resistant to natural biotransformation [125]. Their removal in water treatment plants is regarded as a significant technological issue to limit the possible harm posed by these chemicals in treated wastewater discharged to aquatic habitats. One of the most promising methods for removing pharmaceuticals from water is adsorption [126]. Due to their low cost and ability to selectively adsorb contaminants, MMT is frequently employed for pharmaceutical decontamination. When cations like sodium or calcium are present, their existence balances the interlayer charge.

Tetracycline (TC) adsorption on Patagonian montmorillonite was investigated by Parolo and colleagues as a function of pH, ionic strength, and TC concentration. Intercalation of molecules into the clay mineral's interlayer gaps results through adsorption, and the adsorbed molecules' conformations are likely to change as a result [43]. The amount of adsorbed TC is significantly influenced by the pH of the aqueous solution. The adsorption was reported to be rather high at low pH (2–4), where significant electrostatic attraction occurs between the dominant positively charged TCH_3^+ and the negatively charged MMT species [43]. Vidal and colleagues investigated the utilization of MMT pillared with SnO_2 for the adsorption of trimethoprim (TMP) and sulfamethoxazole (SMX) [127]. When solar-simulated light was applied in the adsorption process, the SnO_2 -Mt sample demonstrated a

greater capacity for TMP adsorption than the unmodified MMT. The unique acid-base and electrostatic interactions of TMP with the Lewis acid sites of SnO_2 were found to be responsible for this effect [127]. In another development, Fu et al. synthesized an environmentally friendly corn cob MMT composite for the single adsorption of ATE. The oxygen-containing functional groups and electrostatic attraction had an impact on the adsorption process. In short, this composite material exhibits excellent development potential for the environmentally friendly adsorption of pharmaceuticals [128]. Imanipoor and colleagues hypothesized a mechanism for protonated L-methionine amino acid-mediated protonated amoxicillin (AMX) adsorption onto modified montmorillonite K10 (MMT K10). Intermolecular interactions supported this mechanism since AMX includes phenol rings, carboxylic ($-\text{COOH}$), amine ($-\text{NH}_2$), and hydroxyl ($-\text{OH}$) functional groups. The L-methionine amino acid contains aliphatic groups, which made the modified MMT K10 organoclay more hydrophobic and increased the clay's interlayer space during synthesis. Therefore, electrostatic interactions, hydrogen bonds, and hydrophobic interactions are responsible for the high adsorption capacity [55]. In another development, Zhang and colleagues reported the use of the Multiwfn wave function in analyzing the adsorption of two b-blockers, atenolol and acebutolol (ATE and ACE) pollutants, on modified MMT with an environmentally friendly cationic surfactant containing an amide group [97]. They used a new, environmentally friendly hexadecanoamide propyl trimethylammonium chloride (NQAS16-3). Figure 4 shows the lowest unoccupied molecular orbital (LUMO) and the highest occupied molecular orbital (HOMO) of three molecules. The lone pair electron of the nitrogen atom in the amide group of NQAS16-3 forms a π - π conjugate with the carbon-oxygen double bond, and Figure 4 showed that the amide group was the focus of the HOMO of NQAS16-3 while the aromatic ring was the primary location of the LUMO of ATE and ACE (especially ATE). As a result, there is a π - π interaction between NQAS16-3 and the two pollutants, which may also be a contributing factor to the enhanced adsorption effect. The aromatic ring of the ACE molecule had one more acetyl substituent than the ATE molecule, and the weaker π - π interaction between N-Mt and ACE was caused by more distributed LUMO [97]. Table 2 presented various findings reported on the application of MMTs for pharmaceutical adsorptions. Information related to the parameter optimizations have been stated, and major findings have been highlighted.

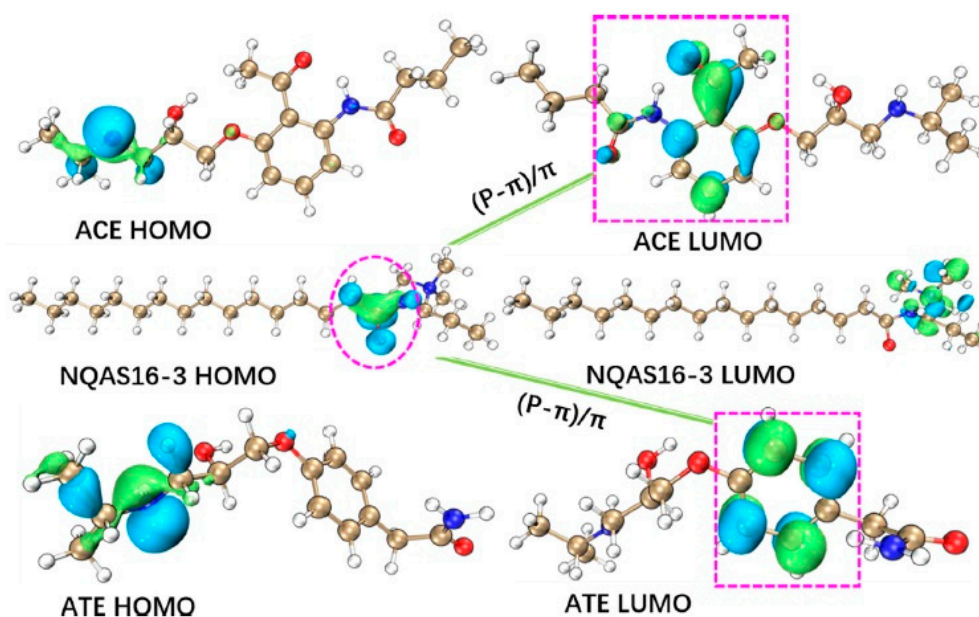


Figure 4. The frontier molecular orbitals for atenolol and acebutolol (ACE and ATE), as well as possible polar interaction between NQAS16-3 and two b-blocker pollutants. Reproduced with permission from Reference [97].

Table 2. Compilation of various MMT and composites for pharmaceuticals adsorption.

Adsorbent	Pollutant	Adsorption Parameters				Highlights	Ref
		pH	Temp (K)	Adsorbate Conc (mg/L)	Contact Time		
Surfactant-MMT	TCS	7	298	0–150	0–60 min	<ul style="list-style-type: none"> - Electrostatic interaction between the gemini surfactant and MMT is responsible for the high adsorption capacity of the adsorbent. - Langmuir model better described the adsorption. 	[56]
MMT-SnO ₂	TMP SMX	-	-	10	24 h	<ul style="list-style-type: none"> - The solar-simulated light enhances the TMP adsorption onto the Mt-SnO₂ when compared to the unmodified clay. 	[127]
DDCAB-MMT	AMP AMX	2–10	298–318	10–180	5–240 min	<ul style="list-style-type: none"> - The adsorption was enhanced by π-π interaction between surfactant and the pollutants, which was confirmed by DFT calculation. - Langmuir model better described the adsorption. 	[129]
MMT	CIP	2–11	298	100	0–144 min	<ul style="list-style-type: none"> - Cation exchange and electrostatic attraction of the MMT dominated the adsorption effect, which resulted in the adsorption sequence of CIP+ > CIP+/- > CIP-. - Langmuir mechanism suited the adsorption process. 	[130]
N-MMT	ACE ATE	3–11	298–318	25–200	5–180 min	<ul style="list-style-type: none"> - The adsorption was influenced by π-π interaction between modifier and pollutant molecules. - Pseudo-second-order and Freundlich models were favored. 	[97]
MMT	TMX	2–5	298	1660	12 h	<ul style="list-style-type: none"> - Cation exchange capacity of the MMT was responsible for the adsorption of the pollutant onto the adsorbent. 	[131]
MoS ₂ /MMT	ACE ATE	3–11	298–318	10–200	0–150 min	<ul style="list-style-type: none"> - The adsorption was enhanced by hydrogen bonding and Van der Waals interaction which occurred more strongly with ATE than ACE. - The adsorption was favored by Langmuir model. 	[132]

Table 2. Cont.

Adsorbent	Pollutant	Adsorption Parameters				Highlights	Ref
		pH	Temp (K)	Adsorbate Conc (mg/L)	Contact Time		
Modified MMT K10	AMX	3.5–11.5	303–333	50–400	10–120 min	<ul style="list-style-type: none"> - The adsorption capacity was higher than the raw clay, attributed to the improvement in cation exchange capacity. - Pseudo-second-order and Langmuir models were favored 	[55]
PVDF/PANI/MMT membrane	TC	2–10	298	100	24 h	<ul style="list-style-type: none"> - The presence of conductive and hydrophilic PANI powders and the high porosity of the MMT in the PVDF membrane reflected the adsorption capacity. - Pseudo-second-order and Langmuir models were favored. 	[133]
C ₁₈ -MMT	IBU 1-OH IBU 2-OH IBU CBX-IBU	-	293	0.5–80	1 h	<ul style="list-style-type: none"> - The higher adsorption capacity of the composite was due to electrostatic interaction and porosity contributed by the C18 modifier. - Pseudo-second-order and Langmuir models were favored 	[134]
MMT- Ti-PILC	AMOX IMP DIF-S PCM	-	298	5–40	24 h	<ul style="list-style-type: none"> - The composite possessed higher BET surface area, microporosity, and acidic sites than the pristine MMT; thus, it has a higher adsorption capacity. - Redlich Peterson model fitted the adsorption data better. 	[22]
Fe ₃ O ₄ /MMT	ENR	3.54–9.73	298	30	0–60 min	<ul style="list-style-type: none"> - The Fe₃O₄/MMT provides sufficient adsorption sites for the ENR molecules due to its higher surface area. 	[135]
MMT	BZ-3	5.5–10.0	278–411	5–250	24 h	<ul style="list-style-type: none"> - The adsorption was due to the higher porosity and cation exchange capacity of the MMT. - Langmuir model fitted the adsorption isotherm best. 	[136]

2.3. MMTs for Heavy Metals and Metal Ions Adsorption

The ecosystem has been known to suffer significantly from the presence of heavy metals in ambient waterways brought on by human activity, the discharge of untreated industrial effluents, and poor sewage disposal practices. Heavy metals are a collection of inorganic chemical species that come from many industries, including tanneries, electroplating, metal polishing, nuclear power plants, and mining operations [137]. Due to their high mobility and lack of biodegradability, heavy metal substances can enter environmental waters through a variety of sources, including soil, landfills, and leachate [138]. The pollutants have negative impacts on aquatic life and are hazardous to both flora and animals [139]. They build up in surface water and are easily transferred into people and animals through the food chain, where they cause serious illnesses such as kidney and liver damage, brain and skin cancer, anemia, pneumonia, hemoglobinuria, stomach dysfunction, diarrhea, and vomiting [140]. Due to their toxicity, the EU and USEPA have identified heavy metals as priority-concerned carcinogenic compounds that must be immediately eliminated [141]. Therefore, a variety of techniques, including physical, biological, and chemical therapies, were used for their rehabilitation. Adsorption, one of the most successful processes, has been thoroughly investigated for heavy metals removal. MMT minerals were effectively used for the adsorption of heavy metals. Because of its reduced cost, lack of toxicity, and high adsorption sites provided by the layered structure compared to other adsorbents, MMT has received much interest in the field of environmental remediation [6]. It is important to modify natural MMT to enhance its adsorption capacity, stability, and other qualities because the features of natural MMT are frequently insufficient for practical applications [104].

Ma and co-workers modified MMT using sodium lignosulfonate (Na-LS) to synthesize lignosulfonate-montmorillonite (LS-MMT). The adsorption capacity (q_e , mg/g) of LS-MMT or Ca/Na-MMT for Pb (II) and Cu (II) at varied reaction intervals demonstrated that LS-MMT has a higher adsorption capacity than Ca/Na-MMT [142]. For the adsorption of heavy metals, mesoporous silica-modified MMT with a grafted chelate ligand was also used [143]. The modified organo-MMT exhibited a high capacity for the adsorption of heavy metal cations. The modification technique described in work can be used as a template for the synthesis of effective adsorbents for usage in contaminated areas [143]. The adsorptive removal of Pb^{2+} and Ni^{2+} ions accommodated in aqueous solutions were evaluated using chitosan/acid-activated MMT composite [144]. The synthesized composite hydrogel has shown effective adsorption of the pollutants at various pH levels via a diffusion mechanism. Variations in the ionic radii and electron affinity increased the adsorption of Ni^{2+} ions to the chitosan/acid-activated MMT [144]. Recently, a composite hydrogel of MoS_2 supported by two-dimensional MMT nanosheets in polyvinyl alcohol ($MoS_2@2D\text{-Mts-PVA Gel}$) was devised and synthesized to increase the hydrophilicity and enable the simple separation of pollutants from water. For the adsorption and separation of metal ions, the $MoS_2@2D\text{ Mts}$ exhibits strong hydrophilicity, and the $MoS_2@2D\text{-Mts-PVA Gel}$ has a porous three-dimensional structure [145]. It was concluded that 2D Mts are the best carriers for loading MoS_2 to interact with polymers and disperse them in water. Adsorption studies showed that the adsorption capacity of $MoS_2@2D\text{-Mts-PVA Gel}$ toward Pb^{2+} increases noticeably when $MoS_2@2D\text{ Mts}$ content and solution pH rise, yielding a high Pb^{2+} adsorption capacity of 257 mg/g. The complexation of Pb^{2+} with S and O atoms on the surface and electrostatic adsorption was suggested as the cause of Pb^{2+} adsorption on MoS_2 [145]. Table 3 summarizes various reports on the application of MMT and its composites for heavy metal adsorption. The parameters conditions have been stated and the overall findings have been stated.

Table 3. Compilation of various HNTs for heavy metals and metal ions adsorption.

Adsorbent	Pollutant	Adsorption Parameters				Highlights	Ref
		pH	Temp (K)	Adsorbate Conc (mg/L)	Contact Time		
LS-MMT Ca/Na-MMT	Cu ²⁺ Pb ²⁺	2–5.5	293–333	50–500	0–60 min	- The LS-MMT has shown higher affinity to the pollutants attributed to the oxygen-containing functional groups present in the lignosulfonate. - It follows the pseudo-second-order and Langmuir model.	[142]
MMT Ca-MMT	Hg ²⁺ , Cr ³⁺ , Pb ²⁺ , Cu ²⁺ , Zn ²⁺ , Ba ²⁺ , Ni ²⁺ , Mn ²⁺ , Cd ²⁺ , Ba ²⁺ , Ag ⁺	1–12	-	50–100	1–16 h	- The Ca-MMT has shown better adsorption efficiency due to its higher cation exchange capacity, which increased with an increased in Ca loading. - The process is favored by pseudo-second-order and Freundlich models.	[146]
MMT Na-MMT Ca-MMT	Pb ²⁺ Cu ²⁺ Cd ²⁺	2–10	298	10–500	15–1440 min	- The Na-MMT and Ca-MMT possessed higher BET surface area and cation exchange capacity, thus displaying higher uptake of the pollutants. - It follows the pseudo-second-order and Langmuir model.	[147]
Silica modified MMT	Zn ²⁺ , Cd ²⁺ , Ni ²⁺ Cu ²⁺ Fe ³⁺ Pb ⁴⁺	3.5	-	5–71	6 h	- The modified MMT displayed high adsorption capacity for the heavy metal cations even in acidic media, attributed to its higher binding for the pollutants due to the chelating agents in the organosilica.	[143]
Fe ₃ O ₄ /MT nanocomposite	Pb ²⁺ , Cu ²⁺ , Ni ²⁺	-	Room Temperature	98–602	40–146 s	- The composite has shown fast adsorption of the pollutants and ease of recovery due to the presence of magnetic Fe ₂ O ₃ . - It follows the pseudo-second-order and Langmuir model.	[148]

Table 3. Cont.

Adsorbent	Pollutant	Adsorption Parameters				Highlights	Ref
		pH	Temp (K)	Adsorbate Conc (mg/L)	Contact Time		
MMT-perlite-iron membrane	As ³⁺	4	297	75–350	43 h	<ul style="list-style-type: none"> - The iron present caused oxidation-reduction reactions with metals observed. - Langmuir gives the best fitting for the isotherm model. 	[149]
Na-MMT	Cd ²⁺ , Cr ²⁺ , Cu ²⁺ , Mn ²⁺ , Ni ²⁺ , Pb ²⁺ , Zn ²⁺	2.5–8	-	-	-	<ul style="list-style-type: none"> - The Na-MMT has higher sorption capacity than the pristine MMT due to the increase in cation exchange capacity caused by the presence of Na. 	[150]
NaF-MMT (rassoul)	Pb ²⁺ , Cd ²⁺ , Hg ²⁺ , Na ₅ P ₃ O ₁₀	3–5	-	-	1 h	<ul style="list-style-type: none"> - The NaF modified the surface property of the MMT to negative form, and the adsorption of heavy metals occurred via electrostatic interaction. 	[151]
F-MMT	Pb ²⁺	-	293–313	100	20–150 min	<ul style="list-style-type: none"> - The Si-O-Mo promoted the charge transfer for the effective adsorption of the pollutant. 	[152]
HLS-MMT	Zn ²⁺ , Pb ²⁺	1–6	298–328	50–300	5–180 min	<ul style="list-style-type: none"> - The loading of HLS on MMT enhanced the adsorption capacity for the Zn²⁺ and Pb²⁺ adsorption. - It follows the pseudo-second-order and Langmuir model. 	[153]
TPP-crosslinked-CTS-modified MMT	Cu ²⁺ , Ni ²⁺	-	283–333	0.5–1	2–60 min	<ul style="list-style-type: none"> - The modified MMT proceeds with higher adsorption capacity due to complexation with CTS and crosslinking agent (TPP). - It follows the pseudo-second-order and Langmuir model. 	[154]

Table 3. Cont.

Adsorbent	Pollutant	Adsorption Parameters				Highlights	Ref
		pH	Temp (K)	Adsorbate Conc (mg/L)	Contact Time		
MoS ₂ @2D-MMT-PVA Gel	Pb ²⁺	2–5	298	0–200	0–480 min	<ul style="list-style-type: none"> - The composite has shown enhanced Pb²⁺ adsorption due to the available adsorption sites on its surface. - It follows the pseudo-second-order and Langmuir model. 	[145]
MMT-Fe ₃ O ₄ -CS	Cr ⁶⁺	3.5–10.6	290–346	0–1100	1 h	<ul style="list-style-type: none"> - The modification enhanced the porosity and ease of recovery of the adsorbent due to Fe₂O₃. - The process follows Langmuir isotherm model. 	[155]
3D MMT hydrogel	Pb ²⁺	2–6	298–308	100–400	3 h	<ul style="list-style-type: none"> - The MMT hydrogel has good filtering performance toward Pb²⁺ adsorption. - It follows the pseudo-second-order and Langmuir model. 	[156]

3. MMT for Photocatalytic Degradation of Pollutants

MMT can undergo surface modification with various species through grafting, immobilization, chemical vapor deposition [73], sol-gel, condensation, surfactant modifications etc., to form exciting surfaces of polymer-MMT composites [114], surfactant/MMT [157], metal//MMT, metal-oxide/MMT nanocomposites [79], for heterogeneous catalysis. Although metal-oxide nanoparticle semiconductors have been the most widely employed photocatalyst due to their low-cost, stability, and ability to generate electrons (e^-) and holes (h^+) generation upon light absorption [158]; however, they suffered extended photo-generated carriers' recombination [159] and can only be excited by ultraviolet radiation. Thus, doping with other materials has been one of the effective ways to improve their performance. The promising properties of MMT, such as high porosity, surface area, good adsorption capacity, potential ion exchange, swelling ability, biocompatibility, and interlayered growth, as well as its low cost and nanostructure, have endowed the material with the potential to form composites with metal-oxide nanoparticles. Thus, the application of the MMT composites for various organic and inorganic pollutants' photocatalytic degradations has been explored.

3.1. MMT for Dyes Degradation

The application of nanostructured MMT materials for dye photocatalytic degradation in environmental waters has been widely explored. Various methods of modification to synthesize catalytically active MMT were evaluated. Modification with organic moieties has been shown to significantly improve the surface properties of MMT for porosity [52], light adsorption, and hydrophobicity as compared to cation exchange and polymer modification. It often resulted in a photocatalyst having properties of the employed organic molecules and that of the nanostructured MMT mineral combined in a single material. This can unquestionably provide answers to certain problems and shortcomings associated with the individual molecules for environmental remediation applications. Thus, organometallic-modified MMT was employed by Mekidiche et al. for the catalytic degradation of cationic dyes. First, the MMT was covalently grafted with 3-aminopropyltriethoxysilane (APTES), forming hydrolyzed MMT surface (K10-APTES) containing NH_2 group, which was modified with triglycine and Fe^{3+} , resulting into K10-APTES-3Gly-Fe catalyst with improved surface area, high crystallinity, and optical adsorption band (around 402–643 nm). The calculated bandgap of the catalyst was 2.03 eV, thereby achieving over 95% degradation of the dye's shortest UV irradiation time of 60 min [10]. The doping of amino acid intercalated Fe onto a surface of MMT has demonstrated good catalytic activity toward the degradation of Reactive Blue (RB 19). The G-Fe-MMT catalyst has shown an effective response to sunlight and effectively worked under neutral pH, achieving 99% degradation efficiency of the cationic dye [160].

The use of metal and metal-oxide nanoparticles in combination with the MMT for photocatalytic activities of dyes have been well reported. The MMT acts majorly as the adsorbent for the trap of the pollutants molecules as well as aid in the effective dispersibility of the photocatalyst. A combination of the materials usually resulted in a photocatalyst with an expandable light response between ultraviolet–visible wavelength ranges [62,90]. Additionally, the photocatalyst bears enhanced photoelectrons and hole separation than the individual metal or metal-oxide nanoparticles [76]. Thus, Xiang et al. examined the application of single and bi-metallic MMT nanocomposites for Rhodamine B (RhB) degradation. The catalysts were prepared via sol-gel methods comprising MMT loaded with Ti and Bi, forming the corresponding Ti-MT and Bi-Ti/MMT nanocomposites. Comparing the optical properties of the two, the latter has a lower bandgap and conduction band than the former. Thus, the lower bandgap (2.3 eV) of the Bi-Ti/MMT has been attributed to its smaller photogenerated carriers' recombination and enhanced e^- and h^+ separation efficiency. Thus, it achieved rapid decolorization of the RhB with a degradation efficiency of over 90%. The photocatalytic activity of the material was tested under visible light irradiation and has shown to be active for continuous degradation of the dye up to four consecutive cycles [85].

TiO₂ was conventionally the most applicable metal-oxide nanoparticle employed as a photocatalyst due to its good semiconducting property and lower cost [65]. However, its inability to absorb light at visible regions and frequent photogenerated recombination have limited its application. Thus, doping the material on the surface of porous organic or inorganic molecules has been a way forward to improve their performance [161]. On this basis, Khataee et al. reported on the Sonocatalytic degradation of basic blue 3 (BB3) dye onto TiO₂-modified MMT synthesized by surface immobilization technique. The resulting TiO₂/MMT composite has shown improved surface area and nanosized surface morphology with particles in the range of 40–60 nm, confirming the successful immobilization of the TiO₂ on the MMT surface. Therefore, a higher dosage (1 g/L) of the catalyst and neutral pH (7.0) of the solution was able to achieve complete degradation of 10 mg/L of the dye within 90 min of the ultrasonication process [74]. Fabrication of plasmonic photocatalyst containing Ag incorporated into Bi₂O₃/MMT for the decomposition of RhB dye under visible light irradiation was reported by Tun and co-workers. The better performance of the Ag-Bi₂O₃/MMT photocatalyst compared to the Bi₂O₃ metal-oxide nanoparticle, pristine MMT, and Bi₂O₃/MMT was attributed to the increased in surface area, visible light absorption, and separation of charged particles upon Ag loading. Thus, complete degradation of the dye was achieved within 60 min (Figure 5a) and followed a pseudo-first-order model (Figure 5b), which increased with the catalyst dosage (Figure 5d). However, it decreased at higher concentrations of the dye (Figure 5e) and the pH (Figure 5c) of the medium [86]. Table S1 summarizes the literature findings reported on the application of MMT composites for dye's photocatalytic degradation. Factors affecting the process were highlighted.

3.2. MMT for Pharmaceuticals Degradation

On the other hand, the use of MMT-modified n-type semiconductor photocatalyst for pharmaceutical decomposition has also been studied. The swelling nature and cationic exchange capacity have been utilized by Tun and co-workers for the preparation of Bi₂O₃/MMT nanocomposite loaded with Ag nanoparticles via the wet impregnation technique. The as-synthesized co-catalyst has shown enhanced plasmonic resonance and visible light response for the degradation of tetracycline (TC). The degradation efficiency was amplified remarkably upon increasing the Ag loading from 3–5 wt.%, attributed to surface area expansion and ease of electron-hole pairs generation and separation. Additionally, changing the catalyst dosage from 0.5 to 1.0 g/L effectively improved the degradation efficiency of the TC from 78% to 90% (Figure 6d) within an irradiation period of 60 min (Figure 6a) [86]. CoFe₂O₄ is a known co-catalyst semiconductor with superior photocatalytic activity toward the generation of charged carriers for the degradation of various pollutants. However, its environmental toxicity and frequent charge recombination has limited its application. On this basis, Wu et al. combined the characteristic property of the material and the non-toxic and enhanced porosity of the MMT for the synthesis of CoFe₂O₄/MMT via hydrothermal technique. The resulting catalyst was activated with persulfate (PS) and peroxymonosulfate (PMS) for the decomposition of carbamazepine (CBZ) via visible light irradiation, recording 93% degradation efficiency in 60 min [70]. The photocatalytic activity of SnO₂ pillared MMT was also investigated toward pharmaceutical degradation. Upon visible light exposure, SMX and TMP concentration was found to decrease, attributed to the adsorption of the molecules onto the SnO₂/MMT surface and the generation of some OH free radicals by the SnO₂ metal-oxide semiconductor [127]. Hassani et al. employed the application of response surface methodology (RSM) for the optimization of CIP degradation using TiO₂-MMT nanocomposite under UV-light irradiation. The good performance of the material was attributed to the higher adsorption sites provided by the MMT, while the TiO₂ served as the powerful oxidizing agent which generated the hydroxyl radicals that attacked the pollutant [67]. Table S2 summarizes the literature findings reported on the application of MMT composites for pharmaceutical photocatalytic degradation. Factors affecting the process were highlighted, and a general remark on each finding was emphasized.

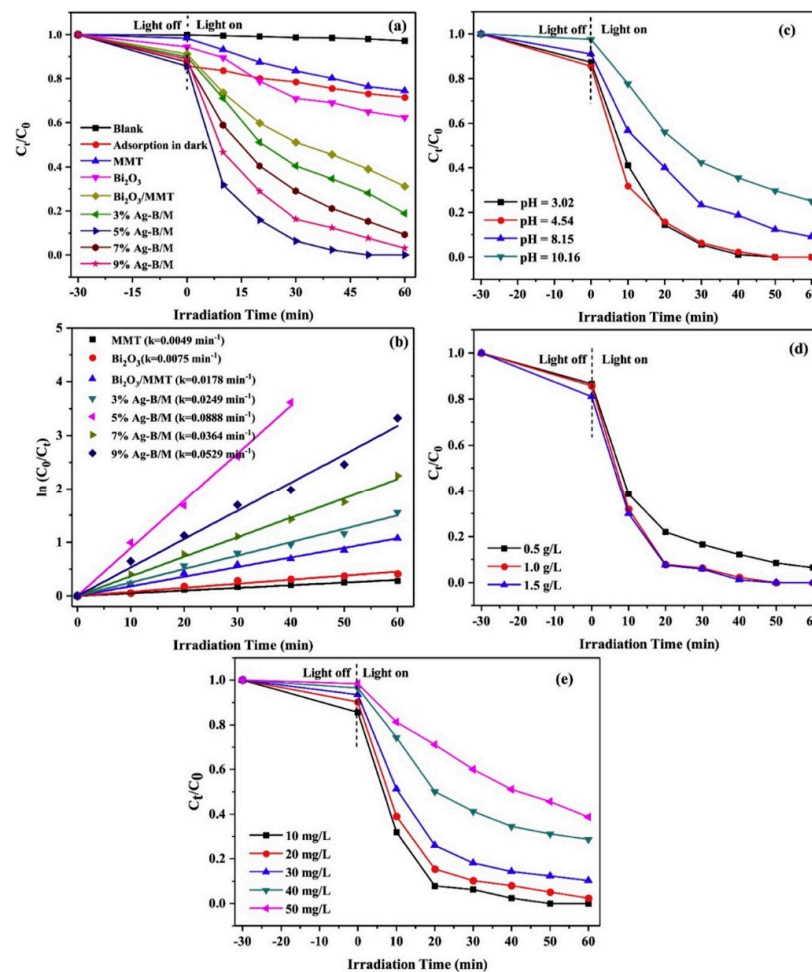


Figure 5. RhB degradation by Ag-B₂O₃/MMT photocatalyst (a) effect of irradiation time (b) kinetics of degradation (c) effect of solution pH (d) dosage of catalyst and (e) effect of initial concentration of the dye. Reproduced with permission from Reference [86].

3.3. MMT for Heavy Metals Degradation

The use of MMT composites for heavy metals photocatalytic degradation was also investigated. Various MMT materials were employed and were able to degrade the inorganic species into non-toxic forms. For instance, Chuaicham et al. reported on the use of double-layered photoactive semiconductors of Zn-Ti in combination with Fe@MMT for the degradation of Cr (VI). The ZTL/Fe@MMT composite has shown good stability to moisture, chemical, and thermal condition and was compatible with UV light. Thus, upon 500 W xenon lamp irradiation, it generated electrons-hole pair with lower recombination rates, which attacked the Cr (VI) molecules and caused its degradation (Figure 7a,b), with excellent efficiency up to five consecutive cycles (Figure 7d) [141]. The MMT functioned as an adsorbent for the pollutant trap and reached adsorption–desorption equilibrium within 30 min. The Fe on the MMT interlayered cavity generated more active electrons, which coincided with the holes on the surface of the Zn-Ti, and this promoted separation of the photogenerated charge carrier [141]. The performance of the composite was better at an alkaline and acidic pH of 3 (Figure 7c). At lower than pH 3, the layered double hydroxide of Zn-Ti gets distorted, which hampers the Cr (III) production. Increasing the photocatalyst loading decreased the photocatalytic efficiency due to the hindrance of light penetration by the turbid solution (Figure 7d). Temperature change did not cause a significant change in the photocatalyst performance (Figure 7f) [141]. Similarly, the degradation of Cr (VI) using MMT-Ag₃PO₄ has been investigated. The photocatalytic activity of the material was promoted by the Ag₃PO₄, which improved the surface porosity of the catalyst and, upon

light irradiation, yielded photo-produced electrons that act on the Cr (VI) molecules. The degradation efficiency was more effective in the presence of citric and phosphoric acids, which generated $\bullet\text{OH}$ radicals [162]. Photocatalytic degradation of Cr (VI) by Fe/MMT composite was also studied. Doping of Fe (III) on the surface of MMT enhanced the photocatalytic activity of the material and achieved 47% degradation of the pollutant within 60 min. Unfortunately, increasing the content of Fe (III) caused a decrease in efficiency by trapping the excited electrons and discouraged the formation of electron-hole pairs. However, adding ethanol as a scavenger significantly enhanced the performance of the photocatalyst through hole formation and promotion of hole-electron pair generation in the medium, thus achieving 100% degradation of the pollutant within 20 min [7].

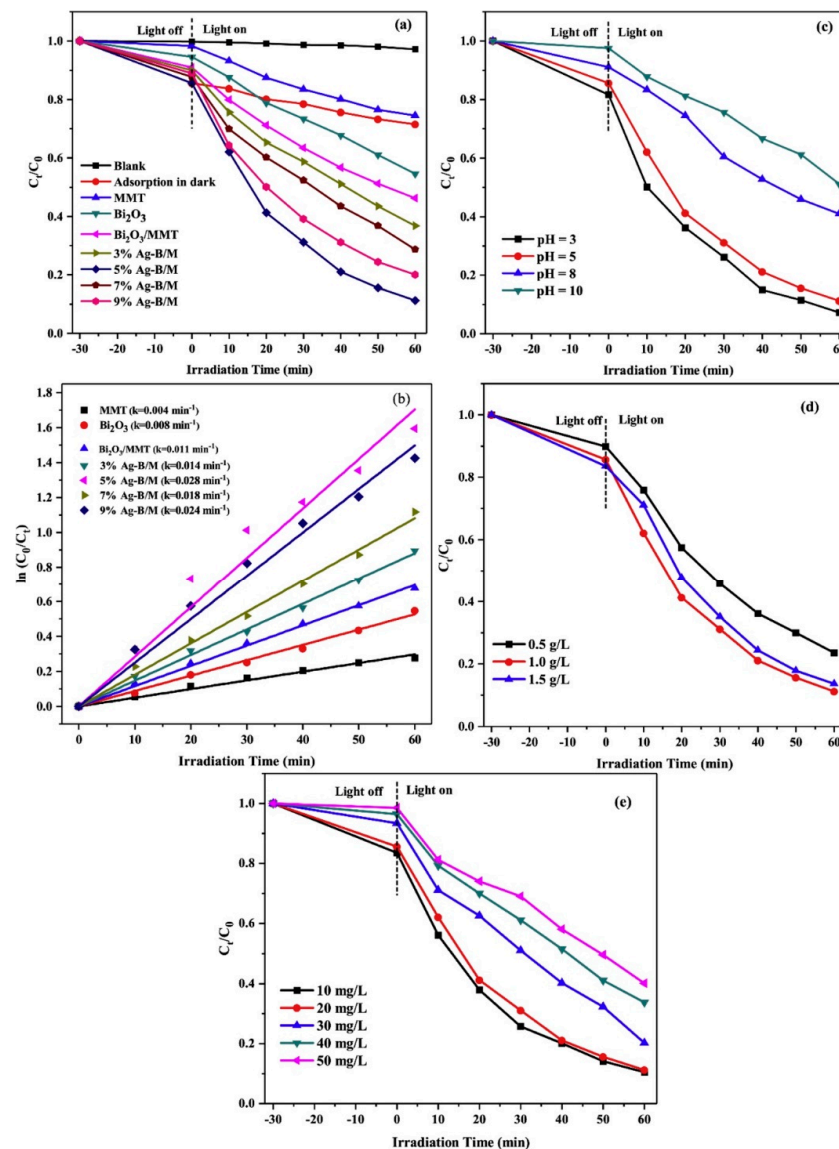


Figure 6. Photocatalytic degradation of TC by Ag-Bi₂O₃/MMT (a) effect of irradiation time, (b) pseudo-first-order reaction rate constant, (c) effect of pH of the solution, (d) effect of catalyst dosages (pH = 3), and (e) effect of initial concentrations. Reproduced with permission from Reference [86].

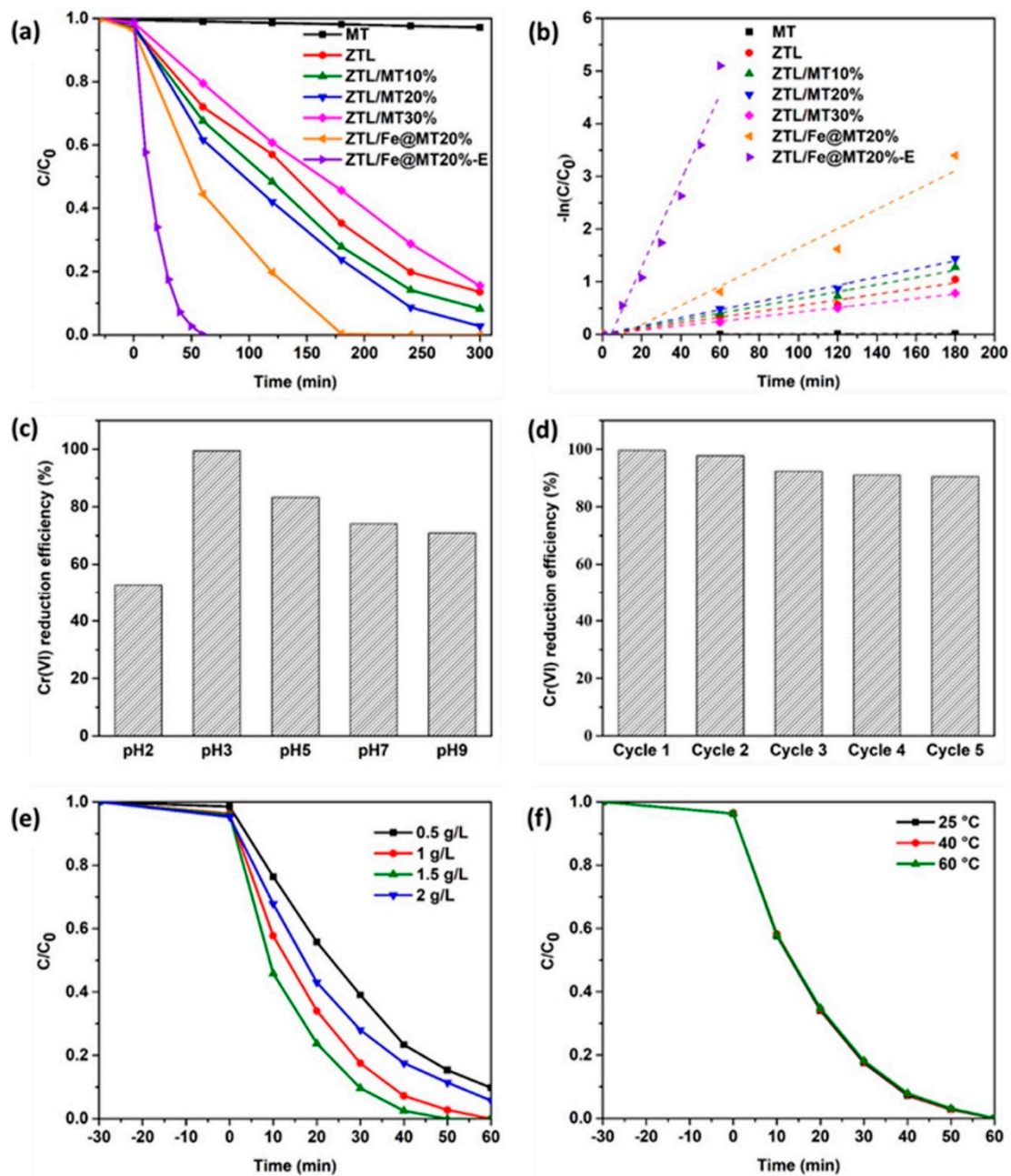


Figure 7. Photocatalytic degradation of Cr (VI) by ZTL/Fe@MMT (a) effect of time, (b) kinetic linear fitting, (c) effect of pH, (d) reusability study, (e) effect of catalyst loading, and (f) effect of temperature. Reproduced with permission from Reference [141].

3.4. Mechanism for Dyes and Pharmaceuticals Photocatalytic Degradation

Researchers have attempted to propose pathways in which the pollutants are degraded by the MMT composites. However, it is noteworthy that all the processes involved adsorption of the pollutants onto the active site of the MMT, followed by the degradation upon the action of the generated free radicals mostly aided by the action of a radiation source, support on the MMT (usually a semi-conducting material or metal nanoparticles, which helps to form the photocatalyst), photo-Fenton reagent, action of reducing agent, sulfate radicals, hydrogen peroxide, and other reactive species [16,84]. Thus, the performance of the photocatalyst lies in the physicochemical characteristic of the composite and its ability to generate photoelectrons and holes with a lower recombination rate. Various

mechanisms have been proposed for the photocatalytic degradation of both cationic and anionic pollutants.

For dyes' photocatalytic degradation, Li et al. have demonstrated that the process proceeds via favorable adsorption of MB molecules onto the surface of the MMT. Upon visible light irradiation, the photocatalyst (MMT-C₃N₄) promoted superoxide peroxide activation and generation of $\bullet\text{O}_2^-$ and h^+ from the solution due to a semi-conducting property of the C₃N₄ which attacks the dye molecules. The MMT-C₃N₄ composite favored the generation of more active species due to its lower photogenerated electron whole pair recombination, resulting in 95% degradation of the MB within 150 min. The degradation rate of the MMT-C₃N₄ composite was 9.2 times in comparison to the pristine C₃N₄ semiconductor [158]. A similar mechanism has been proposed for the photocatalytic degradation of RhB by MMT-SnO₂ nanocomposites. However, the material has shown better performance, with up to 98% degradation efficiency [75]. For further comprehension of the dye degradation mechanisms, Zhao and co-workers proposed that MB was eliminated in two ways on Fe-CS/MMTNS in the presence of H₂O₂ under visible light irradiation (Figure 3). The first involved MB being directly exposed to photo-Fenton degradation and being oxidized into inorganics in aqueous medium. The second involved MB being adsorbed by Fe-CS/MMTNS and being oxidized after that. In other words, MB was eliminated using a combination of photo-Fenton and adsorption. Since Cl was quickly ionized and removed from the chromophore. MB initially had a positive charge and an atomic weight of 284 g/mol. The other part of the MB was first adsorbed by Fe-CS/MMTNS gel and S was oxidized into S = O, followed by its desorption, which was then captured and degraded by the reactive radicals once more. The reactive radicals then directly attacked part of the MB and gradually converted it into inorganic substances like NO₃⁻, SO₂²⁻, and CO₂. Those intermediates were eventually transformed into inorganic materials, and the adsorption sites were renewed for MB adsorption [116].

Similarly, for pharmaceutical phenols photocatalytic degradation, mechanisms for the process have been explored. Wu and co-workers proposed the mechanism for CBZ degradation using nCoFe₂O₄ supported-MMT. Peroxymonosulfate (PMS) generated the SO₄⁻ and $\bullet\text{OH}$, which had been identified as the active radicals for the degradation. The result from x-ray photoelectron spectroscopy (XPS) revealed that the active ions present in the photocatalyst were Co²⁺/Co³⁺ and Fe²⁺/Fe³⁺, and they were responsible for the activation of the PMS. Thus, the active radicals were able to attack the CBZ molecules from the solution, causing ring cleavage and its breakdown, achieving over 90% degradation within 10 min (Figure S1). The process was found to be more effective at lower pH and higher PMS concentrations [70]. Before, Hassaini et al. explored the mechanism for the MET, CIP, and APAP degradation using TiO₂-MMT. The degradation was associated with the adsorption of the pharmaceuticals on the surface of the MMT, followed by the degradation via free radical's attack on the parent ring. Increasing the concentration of ozone resulted in free radical formation by the immobilized TiO₂ upon visible light irradiation, which in turn led to an increase in the efficiency of the process [13]. The pathway for the catalytic activity of Fe²⁺-MMT toward the degradation of SMX was also reported by Shahidi et al. MMT does contribute not only to the adsorption of the SMX but also to the exchangeable site for the photocatalytic reaction. The Fe²⁺ acted as a free cation in the vicinity of the MMT, which activated the photoelectrons from the ozone that attacked the benzene ring of the pollutant. The process proceeds via intermediates formation, which undergoes further degradation to form CO₂ and H₂O as the final degradation products [78].

Photocatalytic degradation of heavy metals by MMT composites was also investigated. Chuaicham et al. proposed the mechanism of Zn-Ti double-layered (ZTL) Fe-MMT nanocomposites for the degradation of Cr (VI). The photocatalyst possessed bandgaps of 3.41 and 3.25 eV for ZTL/MMT and ZTL/Fe-MMT, respectively; thus, the latter has demonstrated better photocatalytic activity. Both ZTL/MMT and ZTL/Fe-MMT were responsive to visible light, thus upon irradiation, ZTL produced photogenerated electrons on the conduction band (CB -1.36 V) and holes from the valence band (VB 1.46 V). However,

the presence of Fe on the surface of the MMT produced more photoexcited electrons which are transferred to the VB of the ZTL because of its higher positive charge. The electron-hole recombination due to Fe and ZTL enhanced the photogenerated charge carrier separation and resulted in higher photocatalytic activity of the composite [141]. The superior performance of MMT-Ag₃O₄ toward the degradation of Cr (VI) was also investigated. MMT has shown good adsorption of pollutants. The Ag₃PO₄ on the interlayers of the MMT possessed negative CB and a smaller bandgap (2.55 eV). As such, under visible light irradiation, it undergoes photosensitization and generates photoexcited electrons, which attack the Cr (VI) molecules, as demonstrated in Figure S2 [162].

4. Prospects and Challenges MMT and Its Composites for the Wastewater Remediation

4.1. Prospects

The overwhelming achievements of MMT and its composites toward pollutant remediation from wastewater are worth mentioning. The adsorption efficiency of the materials for the removal of pollutants was exceptionally high, attributed to their high surface porosity of the material and their good stability toward harsh chemical, moisture, and thermal conditions. They have also shown good mechanical strength and low expansion coefficients. MMT and its composites exhibited good selectivity and catalytic activity for contaminants elimination from wastewater. The materials have performed wonderfully toward dyes, pharmaceuticals, heavy metals, and other organic and inorganic contaminants remediation. Electrostatic attractions, hydrogen, and van der Waals bond formations play a vital role in their interaction with organic and inorganic pollutants. The interaction is due to the presence of silanol groups on the surface of the MMT, and perhaps the negative or positive charge on the surface of the pollutants contributed to the binding interactions.

For the photocatalytic application, composites of the MMT have proven to be effective. MMT formed heterojunctions with various functionalities via its interlayer spacing which allows for the inclusion of molecules, particularly as a support for semiconducting metal and metal oxide nanoparticles. Researchers have thus explored various synthesis routes for the growth of metal and metal oxide nanoparticles on the surface of the MMT. The composites of MMT with these materials are often responsive to light and, upon irradiation, generate photoexcited electrons and holes which act on the pollutants for photocatalytic decomposition. The MMT also provided sufficient adsorption sites for trapping pollutant molecules, a prerequisite to photocatalysis. The layered double hydroxides of the MMT together with the light-assisted adsorption of the support, are well utilized by the catalyst for the photocatalytic degradation activities. Thus, the composites of MMT with metal and metal oxide nanoparticles have shown promising applications for dyes, pharmaceuticals, and heavy metals photocatalytic degradations. Of the metal and metal oxide, those containing iron are more suitable due to their relative abundance, low cost, and their ability to form a composite with MMT with lower bandgap and higher adsorption sites for effective photocatalytic performance.

4.2. Challenges

Apart from the overwhelming success, MMT has some challenges for its application in environmental remediation. Despite its abundant availability, mostly the pristine form suffered lower adsorption capacity for the uptake of various pollutants. Moreover, its surface has an overall negative charge due to the lamella construction of the octahedral silica sheets, resulting in a hydrophobic character and poor interaction with anionic molecules. Additionally, the hydrophilic and oleophobic properties of MMT have been disadvantageous in the elimination of anionic contaminants from the aqueous medium. Moreover, MMT does not possess semiconducting properties; as such, the pristine form cannot be utilized for photocatalytic application. The MMT composite with metal and metal-oxide nanoparticles is mostly desired for such applications.

In most cases, surface modification of the MMT is necessary to achieve higher adsorption capacity catalytic property for the elimination of contaminants from wastewater.

However, modification is often costly and involves using toxic reagents and solvents that do not align with the principle of green chemistry. Moreover, some modification techniques are multi-step and involve the consumption of energy. Thus, it is economically disadvantageous. Often, composites of MMT with inorganic polymers suffered poor incompatibility and a decrease in inherent mechanical strength. Additionally, the matrix effect is often observed when MMT-polymer composites are exposed to high temperatures, causing plasticization and debonding of interfacial tension associated with premature failure of the composite structure. Moreover, some of the MMT-polymer composites result in secondary contamination and pose environmental toxicity to microorganisms, particularly in wastewater remediation applications.

4.3. Conclusions

MMT as a mesoporous clay mineral has been well researched. The availability of MMT deposits in various regions of the planet has made the exploration of the materials possible for various applications. Much attention on the material has been aroused from its low-cost and physicochemical properties such as good dispersibility, surface porosity, good mechanical stability, high moisture, chemical and thermal stability, good cation exchange capacity, and hydrophilicity. The materials offer a good alternative for economic and sustainable applications. MMT has been investigated in material science and engineering for energy generation, air purification, carbon capture, biological processes, water treatments, etc. In the field of wastewater remediation. Good porosity, high stability in the aqueous medium, and good cation exchange capacity have been emphasized. They have been employed for the adsorption and catalytic elimination of various organic and inorganic contaminants, such as dyes, pharmaceuticals, and heavy metals from wastewater.

Modification of MMT has been a way forward to improve its performance for environmental remediation applications. Various strategies have been explored for modification and functionalization. Modifiers include metal and metal-oxide nanoparticles, surfactants, and polymers. They were shown to improve the surface properties of the MMT by enhancing its porosity, cation exchange capacity, mechanical strength, and moisture stability. Apart from that, surface functionalization has been shown to adorn and endure the MMT with semiconducting features for catalytic elimination applications. Thus, composites of MMTs have been explored for contaminant adsorption and photocatalytic elimination. The composites have also been shown to possess a good potential for regeneration and reusability, which is advantageous from an economic point of view. The MMT composites with magnetic metal-oxide nanoparticles have shown the best performance as both adsorbents and photocatalysts for the elimination of contaminants from wastewater. Thus, MMT's composites could serve as futuristic material for environmental remediation applications.

Supplementary Materials: The following supporting information can be downloaded at: <https://www.mdpi.com/article/10.3390/su142416441/s1>.

Author Contributions: Conceptualization, Z.U.Z.; validation, Z.U.Z. and J.-W.L.; formal analysis, Z.N.G.; investigation, Z.N.G.; resources, F.U.; data curation, J.-W.L.; writing—original draft preparation, Z.U.Z. and A.G.; writing—review and editing, M.U.Z.; visualization, F.U.; supervision, J.-W.L.; project administration, Z.U.Z.; funding acquisition, J.-W.L.; All authors have read and agreed to the published version of the manuscript.

Funding: This research received no external funding.

Institutional Review Board Statement: Not applicable.

Informed Consent Statement: Not applicable.

Data Availability Statement: No data has been reported.

Acknowledgments: The authors extend appreciation to the Institute of Semi-Arid Zone Studies, Al-Qalam University Katsina.

Conflicts of Interest: The authors declare no conflict of interest.

References

1. Ningthoujam, R.; Singh, Y.D.; Babu, P.J.; Tirkey, A.; Pradhan, S.; Sarma, M. Nanocatalyst in remediating environmental pollutants. *Chem. Phys. Impact* **2022**, *4*, 100064. [[CrossRef](#)]
2. Castaldo, R.; Avolio, R.; Cocca, M.; Errico, M.E.; Lavorgna, M.; Šalplachta, J.; Santillo, C.; Gentile, G. Hierarchically porous hydrogels and aerogels based on reduced graphene oxide, montmorillonite and hyper-crosslinked resins for water and air remediation. *Chem. Eng. J.* **2022**, *430*, 133162. [[CrossRef](#)]
3. Han, H.; Rafiq, M.K.; Zhou, T.; Xu, R.; Mašek, O.; Li, X. A critical review of clay-based composites with enhanced adsorption performance for metal and organic pollutants. *J. Hazard. Mater.* **2019**, *369*, 780–796. [[CrossRef](#)] [[PubMed](#)]
4. Wang, Y.; Gong, Y.; Lin, N.; Jiang, H.; Wei, X.; Liu, N.; Zhang, X. Cellulose hydrogel coated nanometer zero-valent iron intercalated montmorillonite (CH-MMT-nFe0) for enhanced reductive removal of Cr (VI): Characterization, performance, and mechanisms. *J. Mol. Liq.* **2022**, *347*, 118355. [[CrossRef](#)]
5. Zhu, R.; Chen, Q.; Zhou, Q.; Xi, Y.; Zhu, J.; He, H. Adsorbents based on montmorillonite for contaminant removal from water: A review. *Appl. Clay Sci.* **2016**, *123*, 239–258. [[CrossRef](#)]
6. Wang, R.; Li, H.; Ge, G.; Dai, N.; Rao, J.; Ran, H.; Zhang, Y. Montmorillonite-based two-dimensional nanocomposites: Preparation and applications. *Molecules* **2021**, *26*, 2521. [[CrossRef](#)]
7. Zhang, L.; Chuaicham, C.; Balakumar, V.; Sasaki, K. Effect of ionic Fe(III) doping on montmorillonite for photocatalytic reduction of Cr(VI) in wastewater. *J. Photochem. Photobiol. A Chem.* **2022**, *429*, 113909. [[CrossRef](#)]
8. Bhoj, Y.; Tharmavaram, M.; Rawtani, D. A comprehensive approach to antifouling strategies in desalination, marine environment, and wastewater treatment. *Chem. Phys. Impact* **2021**, *2*, 100008. [[CrossRef](#)]
9. Amaly, N.; El-moghazy, A.Y.; Nitin, N.; Sun, G.; Pandey, P.K. Synergistic adsorption—Photocatalytic degradation of tetracycline by microcrystalline cellulose composite aerogel doped with montmorillonite hosted methylene blue. *Chem. Eng. J.* **2022**, *430*, 133077. [[CrossRef](#)]
10. Mekidiche, M.; Khaldi, K.; Nacer, A.; Boudjema, S.; Ameer, N.; Lerari-zinai, D.; Bachari, K.; Choukchou-braham, A. Organometallic modified montmorillonite application in the wastewater purification: Pollutant photodegradation and antibacterial efficiencies. *Appl. Surf. Sci.* **2021**, *569*, 151097. [[CrossRef](#)]
11. Jagaba, A.H.; Abubakar, S.; Lawal, I.M.; Latiff, A.A.A.; Umaru, I. Wastewater Treatment Using Alum, the Combinations of Alum-Ferric Chloride, Alum-Chitosan, Alum-Zeolite and Alum-Moringa Oleifera as Adsorbent and Coagulant. *Int. J. Eng. Manag.* **2018**, *2*, 67. [[CrossRef](#)]
12. Jagaba, A.; Kutty, S.; Hayder, G.; Latiff, A.; Aziz, N.; Umaru, I.; Ghaleb, A.; Abubakar, S.; Lawal, I.; Nasara, M. Sustainable use of natural and chemical coagulants for contaminants removal from palm oil mill effluent: A comparative analysis. *Ain Shams Eng. J.* **2020**, *11*, 951–960. [[CrossRef](#)]
13. Hassani, A.; Khataee, A.; Karaca, S.; Fathinia, M. Degradation of mixture of three pharmaceuticals by photocatalytic ozonation in the presence of TiO₂/montmorillonite nanocomposite: Simultaneous determination and intermediates identification. *J. Environ. Chem. Eng.* **2017**, *5*, 1964–1976. [[CrossRef](#)]
14. Imam, S.S.; Zango, Z.U. Magnetic Nanoparticle (Fe₃O₄) Impregnated onto Coconut Shell Activated Carbon for the Removal of Ni (II) from Aqueous Solution. *Int. J. Res. Chem. Environ.* **2018**, *8*, 9–15.
15. Isiyaka, H.A.; Jumbri, K.; Sambudi, N.S.; Zango, Z.U.; Abdullah, N.A.F.B.; Saad, B. Effective adsorption of metolachlor herbicide by MIL-53(Al) metal-organic framework: Optimization, validation and molecular docking simulation studies. *Environ. Nanotechnol. Monit. Manag.* **2022**, *18*, 100663. [[CrossRef](#)]
16. Pronk, W.; Ding, A.; Morgenroth, E.; Derlon, N.; Desmond, P.; Burkhardt, M.; Wu, B.; Fane, A.G. Gravity-driven membrane filtration for water and wastewater treatment: A review. *Water Res.* **2019**, *149*, 553–565. [[CrossRef](#)] [[PubMed](#)]
17. Liu, C.J.; Mckay, G.; Jiang, D.; Tenorio, R.; Cath, J.T.; Amador, C.; Murray, C.C.; Brown, J.B.; Wright, H.B.; Schaefer, C.; et al. Pilot-scale field demonstration of a hybrid nanofiltration and UV-sulfite treatment train for groundwater contaminated by per- and polyfluoroalkyl substances (PFASs). *Water Res.* **2021**, *205*, 117677. [[CrossRef](#)]
18. Ali, I.; Kon, T.; Kasianov, V.; Rysev, A.; Panglisch, S.; Mbianda, X.Y.; Habila, M.A.; Almasoud, N. Preparation and characterization of nano-structured modified montmorillonite for dioxidine antibacterial drug removal in water. *J. Mol. Liq.* **2021**, *331*, 115770. [[CrossRef](#)]
19. Bhoj, Y.; Pandey, G.; Bhoj, A.; Tharmavaram, M.; Rawtani, D. Recent advancements in practices related to desalination by means of nanotechnology. *Chem. Phys. Impact* **2021**, *2*, 100025. [[CrossRef](#)]
20. Fouda-Mbanga, B.G.; Prabakaran, E.; Pillay, K. Cd²⁺ ion adsorption and re-use of spent adsorbent with N-doped carbon nanoparticles coated on cerium oxide nanorods nanocomposite for fingerprint detection. *Chem. Phys. Impact* **2022**, *5*, 100083. [[CrossRef](#)]
21. Afzan, M.; Shima, S.M.; Uba, Z.Z.; Ubaidah, N.T.; Bahruddin, S. Adsorption of bisphenol A: Characterisation of ZIF-8, UiO-66(Zr) and MIL-88(Fe) metal-organic frameworks (MOFs). *AIP Conf. Proc.* **2022**, *2454*, 050038. [[CrossRef](#)]
22. Chauhan, M.; Saini, V.K.; Suthar, S. Ti-pillared montmorillonite clay for adsorptive removal of amoxicillin, imipramine, diclofenac-sodium, and paracetamol from water. *J. Hazard. Mater.* **2020**, *399*, 122832. [[CrossRef](#)] [[PubMed](#)]
23. Hernández-Hernández, K.A.; Illescas, J.; del Carmen Díaz-Nava, M.; Martínez-Gallegos, S.; Muro-Urista, C.; Ortega-Aguilar, R.E.; Rodríguez-Alba, E.; Rivera, E. Preparation of nanocomposites for the removal of phenolic compounds from aqueous solutions. *Appl. Clay Sci.* **2018**, *157*, 212–217. [[CrossRef](#)]

24. David, J.P.P. Review on the Preparation, Structure and Property Relation of Clay-Based Polymer Nanocomposites. *Kimika* **2017**, *28*, 44–56. [[CrossRef](#)]
25. Zango, Z.U.; Abu Bakar, N.H.H.; Tan, W.L.; Bakar, M.A. Enhanced removal efficiency of methyl red via the modification of halloysite nanotubes by copper oxide. *J. Dispers. Sci. Technol.* **2017**, *39*, 148–154. [[CrossRef](#)]
26. Krstić, V.; Urošević, T.; Pešovski, B. A review on adsorbents for treatment of water and wastewaters containing copper ions. *Chem. Eng. Sci.* **2018**, *192*, 273–287. [[CrossRef](#)]
27. Huang, J.; Liu, H.; Chen, S.; Ding, C. Hierarchical porous MWCNTs-silica aerogel synthesis for high-efficiency oily water treatment. *J. Environ. Chem. Eng.* **2016**, *4*, 3274–3282. [[CrossRef](#)]
28. Rivero, M.J.; Ribao, P.; Gomez-ruiz, B.; Urtiaga, A.; Ortiz, I. Comparative performance of TiO₂-rGO photocatalyst in the degradation of dichloroacetic and perfluorooctanoic acids. *Sep. Purif. Technol.* **2020**, *240*, 116637. [[CrossRef](#)]
29. Di, Z.; Shen, H.; Guo, Y.; Guo, X.; Kang, B.; Guo, M.; Wei, Y.; Jia, J.; Zhang, R. Heteroatom doping effect of Pt/rGO catalysts for formaldehyde abatement at ambient temperature. *Chem. Phys. Impact* **2022**, *5*, 100103. [[CrossRef](#)]
30. Zango, Z.U.; Sambudi, N.S.; Jumbri, K.; Abu Bakar, N.H.H.; Saad, B. Removal of Pyrene from Aqueous Solution Using Fe-based Metal-organic Frameworks. *IOP Conf. Ser. Earth Environ. Sci.* **2020**, *549*, 012061. [[CrossRef](#)]
31. Zhang, H.; Shi, M.; Ma, J.; Xia, M.; Wang, F.; Liao, C. The interaction and mechanism between threonine-montmorillonite composite and Pb²⁺ or Cu²⁺: Experimental study and theory calculation. *J. Mol. Liq.* **2021**, *326*, 115243. [[CrossRef](#)]
32. Barde, R.V.; Nemade, K.R.; Waghuley, S.A. Optimization of supercapacitive properties of polyindole by dispersion of MnO₂ nanoparticles. *Chem. Phys. Impact* **2022**, *5*, 100100. [[CrossRef](#)]
33. Pontes, J.M.; Azevedo, S. Structural, electronic, and optical properties of the PAI-BN monolayer: A first-principles study. *Chem. Phys. Impact* **2022**, *4*, 100074. [[CrossRef](#)]
34. Hui, W.; Guodong, S.; Xiaoshu, Z.; Wei, Z.; Lin, H.; Ying, Y. In-situ synthesis of TiO₂ rutile/anatase heterostructure by DC magnetron sputtering at room temperature and thickness effect of outermost rutile layer on photocatalysis. *J. Environ. Sci.* **2017**, *60*, 33–42. [[CrossRef](#)]
35. Tiwari, M.; Ramachandran, C.N. Density functional studies of the catalytic oxidation of CO using small aurocarbons. *Chem. Phys. Impact* **2021**, *2*, 100023. [[CrossRef](#)]
36. Damardji, B.; Khalaf, H.; Duclaux, L.; David, B. Preparation of TiO₂-pillared montmorillonite as photocatalyst Part I. Microwave calcination, characterisation, and adsorption of a textile azo dye. *Appl. Clay Sci.* **2009**, *44*, 201–205. [[CrossRef](#)]
37. Daware, K.D.; Shinde, R.N.; Khedkar, C.V.; Patil, S.I.; Pandey, A.K.; Ashokkumar, M.; Gosavi, S.W. Enhanced catalytic activity of platinum decorated silica nanocrystals in rapid reduction of organic dyes. *Chem. Phys. Impact* **2022**, *5*, 100109. [[CrossRef](#)]
38. Jung, C.; Son, A.; Her, N.; Zoh, K.D.; Cho, J.; Yoon, Y. Removal of endocrine disrupting compounds, pharmaceuticals, and personal care products in water using carbon nanotubes: A review. *J. Ind. Eng. Chem.* **2015**, *27*, 1–11. [[CrossRef](#)]
39. Isiyaka, H.A.; Jumbri, K.; Sambudi, N.S.; Zango, Z.U.; Abdullah, N.A.F.B.; Saad, B. Optimizations and docking simulation study for metolachlor adsorption from water onto MIL-101(Cr) metal-organic framework. *Int. J. Environ. Sci. Technol.* **2022**, *101*, 1–16. [[CrossRef](#)]
40. Preetha, B.K.; Vishalakshi, B. Microwave assisted synthesis of karaya gum based montmorillonite nanocomposite: Characterisation, swelling and dye adsorption studies. *Int. J. Biol. Macromol.* **2020**, *154*, 739–750. [[CrossRef](#)]
41. Akyuz, S.; Akyuz, T. Investigation of adsorption of 5-Chlorouracil onto montmorillonite: An IR and Raman spectroscopic study. *Appl. Clay Sci.* **2018**, *164*, 54–57. [[CrossRef](#)]
42. Moretti, C.J.; Das, D.; Kistner, B.T.; Gullicks, H.; Hung, Y.-T. Activated Sludge and Other Aerobic Suspended Culture Processes. *Water* **2011**, *3*, 806–818. [[CrossRef](#)]
43. Parolo, M.E.; Savini, M.C.; Vallés, J.M.; Baschini, M.T.; Avena, M.J. Tetracycline adsorption on montmorillonite: pH and ionic strength effects. *Appl. Clay Sci.* **2008**, *40*, 179–186. [[CrossRef](#)]
44. Unuabonah, E.I.; Ugwuja, C.G.; Omorogie, M.O.; Adewuyi, A.; Oladoja, N.A. Clays for Efficient Disinfection of Bacteria in Water. *Appl. Clay Sci.* **2018**, *151*, 211–223. [[CrossRef](#)]
45. Huang, L.; Huang, X.; Yan, J.; Liu, Y.; Jiang, H.; Zhang, H.; Tang, J.; Liu, Q. Research progresses on the application of perovskite in adsorption and photocatalytic removal of water pollutants. *J. Hazard. Mater.* **2023**, *442*, 130024. [[CrossRef](#)] [[PubMed](#)]
46. Unuabonah, E.I.; Taubert, A. Clay-polymer nanocomposites (CPNs): Adsorbents of the future for water treatment. *Appl. Clay Sci.* **2014**, *99*, 83–92. [[CrossRef](#)]
47. Tabana, L.; Tichapondwa, S.; Labuschagne, F.; Chirwa, E. Adsorption of phenol from wastewater using calcined magnesium-zinc-aluminium layered double hydroxide clay. *Sustainability* **2020**, *12*, 4273. [[CrossRef](#)]
48. Natsir, M.; Putri, Y.I.; Wibowo, D.; Maulidiyah, M.; Salim, L.O.A.; Azis, T.; Bijang, C.M.; Mustapa, F.; Irwan, I.; Arham, Z.; et al. Effects of Ni-TiO₂ Pillared Clay-Montmorillonite Composites for Photocatalytic Enhancement Against Reactive Orange Under Visible Light. *J. Inorg. Organomet. Polym. Mater.* **2021**, *31*, 3378–3388. [[CrossRef](#)]
49. Zeng, G.; He, Y.; Zhan, Y.; Zhang, L.; Pan, Y.; Zhang, C.; Yu, Z. Novel polyvinylidene fluoride nanofiltration membrane blended with functionalized halloysite nanotubes for dye and heavy metal ions removal. *J. Hazard. Mater.* **2016**, *317*, 60–72. [[CrossRef](#)]
50. Lazaratou, C.V.; Panagiotaras, D.; Panagopoulos, G.; Pospíšil, M.; Papoulis, D. Ca treated Palygorskite and Halloysite clay minerals for Ferrous Iron (Fe²⁺) removal from water systems. *Environ. Technol. Innov.* **2020**, *19*, 100961. [[CrossRef](#)]
51. Xu, W.; Qin, H.; Zhu, J.; Johnson, T.M.; Tan, D.; Liu, C.; Takahashi, Y. Selenium isotope fractionation during adsorption onto montmorillonite and kaolinite. *Appl. Clay Sci.* **2021**, *211*, 106189. [[CrossRef](#)]

52. Goswami, M.; Das, A.M. Synthesis and characterization of a biodegradable Cellulose acetate-montmorillonite composite for effective adsorption of Eosin Y. *Carbohydr. Polym.* **2019**, *206*, 863–872. [[CrossRef](#)] [[PubMed](#)]
53. Bee, S.L.; Abdullah, M.A.A.; Bee, S.T.; Sin, L.T.; Rahmat, A.R. Polymer nanocomposites based on silylated-montmorillonite: A review. *Prog. Polym. Sci.* **2018**, *85*, 57–82. [[CrossRef](#)]
54. Fernández Solarte, A.M.; Villarroel-Rocha, J.; Morantes, C.F.; Montes, M.L.; Sapag, K.; Curutchet, G.; Torres Sánchez, R.M. Insight into surface and structural changes of montmorillonite and organomontmorillonites loaded with Ag. *Comptes Rendus Chim.* **2019**, *22*, 142–153. [[CrossRef](#)]
55. Imanipoor, J.; Ghafelebashi, A.; Mohammadi, M.; Dinari, M.; Ehsani, M.R. Fast and effective adsorption of amoxicillin from aqueous solutions by L-methionine modified montmorillonite K10. *Colloids Surf. A Physicochem. Eng. Asp.* **2021**, *611*, 125792. [[CrossRef](#)]
56. Liu, B.; Lu, J.; Xie, Y.; Yang, B.; Wang, X.; Sun, R. Microwave-assisted modification on montmorillonite with ester-containing Gemini surfactant and its adsorption behavior for triclosan. *J. Colloid Interface Sci.* **2014**, *418*, 311–316. [[CrossRef](#)]
57. Cheira, M.F.; Kouraim, M.N.; Zidan, I.H.; Mohamed, W.S.; Hassanein, T.F. Adsorption of U(VI) from sulfate solution using montmorillonite/polyamide and nano-titanium oxide/polyamide nanocomposites. *J. Environ. Chem. Eng.* **2020**, *8*, 104427. [[CrossRef](#)]
58. Xu, C.; Wu, H.; Gu, F.L. Efficient adsorption and photocatalytic degradation of Rhodamine B under visible light irradiation over BiOBr/montmorillonite composites. *J. Hazard. Mater.* **2014**, *275*, 185–192. [[CrossRef](#)]
59. He, Y.; Jiang, D.B.; Chen, J.; Zhang, Y.X. Synthesis of MnO₂ nanosheets on montmorillonite for oxidative degradation and adsorption of methylene blue. *J. Colloid Interface Sci.* **2018**, *510*, 207–220. [[CrossRef](#)]
60. Guz, L.; Curutchet, G.; Sanchez, R.M.T.; Candal, R. Adsorption of crystal violet on montmorillonite (or iron modified montmorillonite) followed by degradation through Fenton or photo-Fenton type reactions. *J. Environ. Chem. Eng.* **2014**, *2*, 2344–2351. [[CrossRef](#)]
61. Bayram, T.; Bucak, S.; Ozturk, D. BR13 dye removal using sodium dodecyl sulfate modified montmorillonite: Equilibrium, thermodynamic, kinetic and reusability studies. *Chem. Eng. Process. Process Intensif.* **2020**, *158*, 108186. [[CrossRef](#)]
62. Vinuth, M.; Naik, H.S.B.; Vinoda, B.M.; Gururaj, H.; Thomas, N.; Arunkumar, G. Enhanced removal of methylene blue dye in aqueous solution using eco-friendly Fe (III)—Montmorillonite. *Mater. Today Proc.* **2017**, *4*, 424–433. [[CrossRef](#)]
63. Chahardahasoumi, S.; Jalali, S.A.H.; Sarvi, M.N. Tetracycline removal enhancement with Fe-saturated nanoporous montmorillonite in a tripartite adsorption/desorption/photo-Fenton degradation process. *Environ. Sci. Pollut. Res.* **2022**, *29*, 57248–57260. [[CrossRef](#)]
64. Foroutan, R.; Mohammadi, R.; MousaKhanloo, F.; Sahebi, S.; Ramavandi, B.; Kumar, P.S.; Vardhan, K.H. Performance of montmorillonite/graphene oxide/CoFe₂O₄ as a magnetic and recyclable nanocomposite for cleaning methyl violet dye-laden wastewater. *Adv. Powder Technol.* **2020**, *31*, 3993–4004. [[CrossRef](#)]
65. Tao, E.; Xiao, X.; Yang, S. A new synthesizing method of TiO₂ with montmorillonite: Effective photoelectron transfer to degrade Rhodamine B. *Sep. Purif. Technol.* **2021**, *258*, 118070. [[CrossRef](#)]
66. Shahabi, H.; Allahrasani, A.; Naghizadeh, A. Photocatalytic degradation of acetaminophen in aqueous solution in the presence of montmorillonite nanosheets modified with titanium dioxide. *Desalin. Water Treat.* **2019**, *149*, 164–170. [[CrossRef](#)]
67. Hassani, A.; Khataee, A.; Karaca, S. Photocatalytic degradation of ciprofloxacin by synthesized TiO₂ nanoparticles on montmorillonite: Effect of operation parameters and artificial neural network modeling. *J. Mol. Catal. A Chem.* **2015**, *409*, 149–161. [[CrossRef](#)]
68. Kiranşan, M.; Khataee, A.; Karaca, S.; Sheydaei, M. Artificial neural network modeling of photocatalytic removal of a disperse dye using synthesized ZnO nanoparticles on montmorillonite. *Spectrochim. Acta Part A Mol. Biomol. Spectrosc.* **2015**, *140*, 465–473. [[CrossRef](#)]
69. Massoudinejad, M.; Paseban, A.; Yazdanbakhsh, A.; Nabid, M.R. Preparation, Characterization, and Application of N,S-codoped TiO₂/Montmorillonite Nanocomposite for the Photocatalytic Degradation of Ciprofloxacin: Optimization by Response Surface Methodology. *Polish J. Chem. Technol.* **2018**, *20*, 66–74. [[CrossRef](#)]
70. Wu, J.; Cagnetta, G.; Wang, B.; Cui, Y.; Deng, S.; Wang, Y.; Huang, J.; Yu, G. Efficient degradation of carbamazepine by organo-montmorillonite supported nCoFe₂O₄-activated peroxydisulfate process. *Chem. Eng. J.* **2019**, *368*, 824–836. [[CrossRef](#)]
71. Peng, K.; Wang, H.; Li, X.; Wang, J.; Xu, L.; Gao, H.; Niu, M.; Ma, M.; Yang, J. One-step hydrothermal growth of MoS₂ nanosheets/CdS nanoparticles heterostructures on montmorillonite for enhanced visible light photocatalytic activity. *Appl. Clay Sci.* **2019**, *175*, 86–93. [[CrossRef](#)]
72. Onwuka, K.E.; Achilike, K.; Eze, K.S.; Enenwa, N.E. Montmorillonite Clay Enhanced TiO₂ Nanoparticle for Photocatalytic Degradation of Organic Pollutants: Mini Review. *Int. J. Pharm. Sci.* **2021**, *1*, 33–38. [[CrossRef](#)]
73. Zhang, J.; Liu, T.; Fu, L.; Ye, G. Synthesis of nanosized ultrathin MoS₂ on montmorillonite nanosheets by CVD method. *Chem. Phys. Lett.* **2021**, *781*, 138972. [[CrossRef](#)]
74. Khataee, A.; Sheydaei, M.; Hassani, A.; Taseidifar, M.; Karaca, S. Sonocatalytic removal of an organic dye using TiO₂/Montmorillonite nanocomposite. *Ultrason. Sonochem.* **2015**, *22*, 404–411. [[CrossRef](#)]
75. Fatimah, I.; Rubiyanto, D.; Sahroni, I.; Putra, R.S.; Nurillahi, R.; Nugraha, J. Physicochemical characteristics and photocatalytic performance of Tin oxide/montmorillonite nanocomposites at various Sn/montmorillonite molar to mass ratios. *Appl. Clay Sci.* **2020**, *193*, 105671. [[CrossRef](#)]

76. Fatimah, I.; Purwiandono, G.; Hidayat, A.; Sagadevan, S.; Kamari, A. Mechanistic insight into the adsorption and photocatalytic activity of a magnetically separable γ -Fe₂O₃/Montmorillonite nanocomposite for rhodamine B removal. *Chem. Phys. Lett.* **2022**, *792*, 139410. [[CrossRef](#)]
77. Zhang, X.; Guo, Y.; Shi, S.; Liu, E.; Li, T.; Wei, S.; Li, Y.; Li, Y.; Sun, G.; Zhao, Z. Efficient and stable iron-copper montmorillonite heterogeneous Fenton catalyst for removing Rhodamine B. *Chem. Phys. Lett.* **2021**, *776*, 138673. [[CrossRef](#)]
78. Shahidi, D.; Moheb, A.; Abbas, R.; Larouk, S.; Roy, R.; Azzouz, A. Total mineralization of sulfamethoxazole and aromatic pollutants through Fe²⁺-montmorillonite catalyzed ozonation. *J. Hazard. Mater.* **2015**, *298*, 338–350. [[CrossRef](#)]
79. González, B.; Trujillano, R.; Vicente, M.A.; Rives, V.; Korili, S.A.; Gil, A. Photocatalytic degradation of trimethoprim on doped Ti-pillared montmorillonite. *Appl. Clay Sci.* **2019**, *167*, 43–49. [[CrossRef](#)]
80. Joseph, A.; Vellayan, K.; González, B.; Vicente, M.A.; Gil, A. Effective degradation of methylene blue in aqueous solution using Pd-supported Cu-doped Ti-pillared montmorillonite catalyst. *Appl. Clay Sci.* **2019**, *168*, 7–10. [[CrossRef](#)]
81. Zhang, H.; Jiang, L.; Wang, H.; Li, Y.; Chen, J.; Li, J.; Guo, H.; Yuan, X.; Xiong, T. Evaluating the remediation potential of MgFe₂O₄-montmorillonite and its co-application with biochar on heavy metal-contaminated soils. *Chemosphere* **2022**, *299*, 134217. [[CrossRef](#)] [[PubMed](#)]
82. Jin, J.; Chen, B.; Liu, L.; Liu, R.; Qian, G.; Wei, H.; Zheng, J. A study on modified bitumen with metal doped nano-TiO₂ pillared montmorillonite. *Materials* **2019**, *12*, 1910. [[CrossRef](#)]
83. Peng, A.; Wang, Y.; Yin, L.; Chen, Z.; Gu, C. Halide salts induced the photodegradation of a fat-burning compound 2,4-dinitrophenol by iron-montmorillonite. *Chemosphere* **2022**, *291*, 132694. [[CrossRef](#)] [[PubMed](#)]
84. Sirajudheen, P.; Meenakshi, S. Lanthanum (III) incorporated chitosan-montmorillonite composite as flexible material for adsorptive removal of azo dyes from water. *Mater. Today Proc.* **2020**, *27*, 318–326. [[CrossRef](#)]
85. Xiang, H.; Tuo, B.; Tian, J.; Hu, K.; Wang, J.; Cheng, J.; Tang, Y. Preparation and photocatalytic properties of Bi-doped TiO₂/montmorillonite composite. *Opt. Mater.* **2021**, *117*, 111137. [[CrossRef](#)]
86. Phyu, P.; Wang, J.; Thinn, T.; Wu, X.; Zhang, G. Fabrication of functionalized plasmonic Ag loaded Bi₂O₃/montmorillonite nanocomposites for efficient photocatalytic removal of antibiotics and organic dyes. *J. Alloys Compd.* **2020**, *818*, 152836. [[CrossRef](#)]
87. Awad, A.M.; Shaikh, S.M.R.; Jalab, R.; Gulied, M.H.; Nasser, M.S.; Benamor, A.; Adham, S. Adsorption of organic pollutants by natural and modified clays: A comprehensive review. *Sep. Purif. Technol.* **2019**, *228*, 115719. [[CrossRef](#)]
88. Chu, Y.; Khan, M.A.; Wang, F.; Xia, M.; Lei, W.; Zhu, S. Kinetics and equilibrium isotherms of adsorption of Pb(II) and Cu(II) onto raw and arginine-modified montmorillonite. *Adv. Powder Technol.* **2019**, *30*, 1067–1078. [[CrossRef](#)]
89. Zhao, M.; Wei, L.; Zheng, Y.; Liu, M.; Wang, J.; Qiu, Y. Structural effect of imidazolium-type ionic liquid adsorption to montmorillonite. *Sci. Total Environ.* **2019**, *666*, 858–864. [[CrossRef](#)]
90. Açıslı, Ö.; Karaca, S.; Gürses, A. Investigation of the alkyl chain lengths of surfactants on their adsorption by montmorillonite (Mt) from aqueous solutions. *Appl. Clay Sci.* **2017**, *142*, 90–99. [[CrossRef](#)]
91. Tabrizi, S.H.; Tanhaei, B.; Ayati, A.; Ranjbari, S. Substantial improvement in the adsorption behavior of montmorillonite toward Tartrazine through hexadecylamine impregnation. *Environ. Res.* **2022**, *204*, 111965. [[CrossRef](#)] [[PubMed](#)]
92. Yang, Q.; Gao, M.; Luo, Z.; Yang, S. Enhanced removal of bisphenol A from aqueous solution by organo-montmorillonites modified with novel Gemini pyridinium surfactants containing long alkyl chain. *Chem. Eng. J.* **2016**, *285*, 27–38. [[CrossRef](#)]
93. Yazdi, F.; Anbia, M.; Salehi, S. Characterization of functionalized chitosan-clinoptilolite nanocomposites for nitrate removal from aqueous media. *Int. J. Biol. Macromol.* **2019**, *130*, 545–555. [[CrossRef](#)] [[PubMed](#)]
94. Eltabey, R.M.; Abdelwahed, F.T.; Eldefrawy, M.M.; Elnagar, M.M. Fabrication of poly(maleic acid)-grafted cross-linked chitosan/montmorillonite nanospheres for ultra-high adsorption of anionic acid yellow-17 and cationic brilliant green dyes in single and binary systems. *J. Hazard. Mater.* **2022**, *439*, 129589. [[CrossRef](#)]
95. Tabana, L.S.; Ledikwa, R.P.; Tichapondwa, S.M. Adsorption of phenol from wastewater using modified layered double hydroxide clay. *Chem. Eng. Trans.* **2019**, *76*, 1267–1272. [[CrossRef](#)]
96. Park, Y.; Ayoko, G.A.; Kurdi, R.; Horváth, E.; Kristóf, J.; Frost, R.L. Adsorption of phenolic compounds by organoclays: Implications for the removal of organic pollutants from aqueous media. *J. Colloid Interface Sci.* **2013**, *406*, 196–208. [[CrossRef](#)]
97. Zhang, H.; Ma, J.; Shi, M.; Xia, M.; Wang, F.; Fu, C. Adsorption of two β -blocker pollutants on modified montmorillonite with environment-friendly cationic surfactant containing amide group: Batch adsorption experiments and Multiwfn wave function analysis. *J. Colloid Interface Sci.* **2021**, *590*, 601–613. [[CrossRef](#)]
98. Xue, G.; Gao, M.; Gu, Z.; Luo, Z.; Hu, Z. The removal of p-nitrophenol from aqueous solutions by adsorption using gemini surfactants modified montmorillonites. *Chem. Eng. J.* **2013**, *218*, 223–231. [[CrossRef](#)]
99. Luo, Z.; Gao, M.; Yang, S.; Yang, Q. Adsorption of phenols on reduced-charge montmorillonites modified by bispyridinium dibromides: Mechanism, kinetics and thermodynamics studies. *Colloids Surf. A Physicochem. Eng. Asp.* **2015**, *482*, 222–230. [[CrossRef](#)]
100. Gopal, K.; Sen, S. Adsorption of a few heavy metals on natural and modified kaolinite and montmorillonite: A review. *Adv. Colloid Interface Sci.* **2008**, *140*, 114–131. [[CrossRef](#)]
101. Dean, K.M.; Do, M.D.; Petinakis, E.; Yu, L. Key interactions in biodegradable thermoplastic starch/poly(vinyl alcohol)/montmorillonite micro- and nanocomposites. *Compos. Sci. Technol.* **2008**, *68*, 1453–1462. [[CrossRef](#)]
102. Krzaczkowska, J.; Strankowski, M.; Jurga, S.; Jurga, K.; Pietraszko, A. NMR dispersion studies of poly(ethylene oxide)/sodium montmorillonite nanocomposites. *J. Non. Cryst. Solids* **2010**, *356*, 945–951. [[CrossRef](#)]

103. Hnamte, M.; Pulikkal, A.K. Clay-polymer nanocomposites for water and wastewater treatment: A comprehensive review. *Chemosphere* **2022**, *307*, 135869. [[CrossRef](#)]
104. Mdallalose, L.; Balogun, M.; Setshedi, K.; Tukulula, M.; Chimuka, L.; Chetty, A. Synthesis, characterization and optimization of poly(p-phenylenediamine)-based organoclay composite for Cr(VI) remediation. *Appl. Clay Sci.* **2017**, *139*, 72–80. [[CrossRef](#)]
105. Fayazi, M.; Ghanbarian, M. One-Pot Hydrothermal Synthesis of Polyethylenimine Functionalized Magnetic Clay for Efficient Removal of Noxious Cr(VI) from Aqueous Solutions. *Silicon* **2020**, *12*, 125–134. [[CrossRef](#)]
106. Mahdavinia, G.R.; Rahmani, Z.; Mosallanezhad, A.; Karami, S.; Shahriari, M. Effect of magnetic laponite RD on swelling and dye adsorption behaviors of κ -carrageenan-based nanocomposite hydrogels. *Desalin. Water Treat.* **2016**, *57*, 20582–20596. [[CrossRef](#)]
107. El-kousy, S.M.; El-shorbagy, H.G.; El-ghaffar, M.A.A. Chitosan/montmorillonite composites for fast removal of methylene blue from aqueous solutions. *Mater. Chem. Phys.* **2020**, *254*, 123236. [[CrossRef](#)]
108. Zhang, M.; Chang, L.; Zhao, Y.; Yu, Z. Fabrication, characterization and adsorption behavior of montmorillonite/polypyrrole nanocomposites for Eosin Y removal. *Polym. Bull.* **2018**, *75*, 4881–4899. [[CrossRef](#)]
109. Amaly, N.; Pandey, P.; El-moghazy, A.Y.; Sun, G.; Pandey, P.K. Cationic microcrystalline cellulose–Montmorillonite composite aerogel for preconcentration of inorganic anions from dairy wastewater. *Talanta* **2022**, *242*, 123281. [[CrossRef](#)]
110. Sun, S.; Xiao, W.; You, C.; Zhou, W.; Garba, Z.N.; Wang, L.; Yuan, Z. Methods for preparing and enhancing photocatalytic activity of basic bismuth nitrate. *J. Clean. Prod.* **2021**, *294*, 126350. [[CrossRef](#)]
111. Zango, Z.U.; Jumbri, K.; Sambudi, N.S.; Bakar, H.H.A.; Garba, Z.N.; Isiyaka, H.A.; Saad, B. Selective adsorption of dyes and pharmaceuticals from water by UiO metal–organic frameworks: A comprehensive review. *Polyhedron* **2021**, *210*, 115515. [[CrossRef](#)]
112. Imam, S.S.; Muhammad, A.I.; Babamale, H.F.; Zango, Z.U. Removal of Orange G Dye from Aqueous Solution by Adsorption: A Short Review. *J. Environ. Treat. Tech.* **2021**, *9*, 318–327. [[CrossRef](#)]
113. Dehghani, M.H.; Zarei, A.; Mesdaghinia, A.; Nabizadeh, R.; Alimohammadi, M.; Afsharnia, M.; McKay, G. Production and application of a treated bentonite–chitosan composite for the efficient removal of humic acid from aqueous solution. *Chem. Eng. Res. Des.* **2018**, *140*, 102–115. [[CrossRef](#)]
114. Minisy, I.M.; Salahuddin, N.A.; Ayad, M.M. Adsorption of methylene blue onto chitosan-montmorillonite/polyaniline nanocomposite. *Appl. Clay Sci.* **2021**, *203*, 105993. [[CrossRef](#)]
115. Yilmazoglu, M.; Turan, B.; Demircivi, P.; Hizal, J. Synthesis and characterization of imidazolium based ionic liquid modified montmorillonite for the adsorption of Orange II dye: Effect of chain length. *J. Mol. Struct.* **2022**, *1249*, 131628. [[CrossRef](#)]
116. Zhao, Y.; Kang, S.; Qin, L.; Wang, W.; Zhang, T.; Song, S.; Komarneni, S. Self-assembled gels of Fe-chitosan/montmorillonite nanosheets: Dye degradation by the synergistic effect of adsorption and photo-Fenton reaction. *Chem. Eng. J.* **2020**, *379*, 122322. [[CrossRef](#)]
117. Wang, C.; Juang, L.; Hsu, T.; Lee, C.; Lee, J.; Huang, F. Adsorption of basic dyes onto montmorillonite. *J. Colloid Interface Sci.* **2004**, *273*, 80–86. [[CrossRef](#)]
118. Ouachtak, H.; El Haouti, R.; El Guerdaoui, A.; Haounati, R.; Amaterz, E.; Addi, A.A.; Akbal, F.; Taha, M.L. Experimental and molecular dynamics simulation study on the adsorption of Rhodamine B dye on magnetic montmorillonite composite γ -Fe₂O₃@Mt. *J. Mol. Liq.* **2020**, *309*, 113142. [[CrossRef](#)]
119. Belbel, A.; Kharroubi, M.; Janot, J.; Abdessamad, M.; Haouzi, A.; Khaldoun, I.; Balme, S. Preparation and characterization of homoionic montmorillonite modified with ionic liquid: Application in dye adsorption. *Colloids Surf. A* **2018**, *558*, 219–227. [[CrossRef](#)]
120. Mahmoodi, N.M.; Taghizadeh, A.; Taghizadeh, M.; Baglou, M.A.S. Surface modified montmorillonite with cationic surfactants: Preparation, characterization, and dye adsorption from aqueous solution. *J. Environ. Chem. Eng.* **2019**, *7*, 103243. [[CrossRef](#)]
121. Jiang, D.B.; Jing, C.; Yuan, Y.; Feng, L.; Liu, X.; Dong, F.; Dong, B.; Zhang, Y.X. 2D-2D growth of NiFe LDH nanoflakes on montmorillonite for cationic and anionic dye adsorption performance. *J. Colloid Interface Sci.* **2019**, *540*, 398–409. [[CrossRef](#)] [[PubMed](#)]
122. Abou, M.F.; Hegazy, D.E.; Ismail, S.A. Radiation synthesis, characterization and dye adsorption of alginate–Organophilic montmorillonite nanocomposite. *Carbohydr. Polym.* **2012**, *87*, 2263–2269. [[CrossRef](#)]
123. Hizal, J.; Yilmazoglu, M.; Kanmaz, N.; Ercag, E. Efficient removal of indigo dye by using sulfonated poly (ether ether ketone) (sPEEK), montmorillonite (MMT) and sPEEK-MMT composites as novel adsorbent. *Chem. Phys. Lett.* **2022**, *794*, 139482. [[CrossRef](#)]
124. Pereira, F.A.R.; Sousa, K.S.; Cavalcanti, G.R.S.; França, D.B.; Queiroga, L.N.F.; Santos, I.M.G.; Fonseca, M.G.; Jaber, M. Green biosorbents based on chitosan-montmorillonite beads for anionic dye removal. *J. Environ. Chem. Eng.* **2017**, *5*, 3309–3318. [[CrossRef](#)]
125. Kyzas, G.Z.; Kostoglou, M. Green adsorbents for wastewaters: A critical review. *Materials* **2014**, *7*, 333–364. [[CrossRef](#)]
126. Laabd, M.; Brahmi, Y.; El Ibrahim, B.; Hsini, A.; Toufik, E.; Abdellaoui, Y.; Oualid, H.A.; El Ouardi, M.; Albourine, A. A novel mesoporous Hydroxyapatite @ Montmorillonite hybrid composite for high-performance removal of emerging Ciprofloxacin antibiotic from water: Integrated experimental and Monte Carlo computational assessment. *J. Mol. Liq.* **2021**, *338*, 116705. [[CrossRef](#)]
127. Vidal, C.B.; dos Santos, A.B.; do Nascimento, R.F.; Bandosz, T.J. Reactive adsorption of pharmaceuticals on tin oxide pillared montmorillonite: Effect of visible light exposure. *Chem. Eng. J.* **2015**, *259*, 865–875. [[CrossRef](#)]

128. Fu, C.; Zhang, H.; Xia, M.; Lei, W.; Wang, F. The single/co-adsorption characteristics and microscopic adsorption mechanism of biochar-montmorillonite composite adsorbent for pharmaceutical emerging organic contaminant atenolol and lead ions. *Ecotoxicol. Environ. Saf.* **2020**, *187*, 109763. [CrossRef]
129. Li, Y.; Shi, M.; Xia, M.; Wang, F. The enhanced adsorption of Ampicillin and Amoxicillin on modified montmorillonite with dodecyl dimethyl benzyl ammonium chloride: Experimental study and density functional theory calculation. *Adv. Powder Technol.* **2021**, *32*, 3465–3475. [CrossRef]
130. Zhang, H.; Zhao, F.; Xia, M.; Wang, F. Microscopic adsorption mechanism of montmorillonite for common ciprofloxacin emerging contaminant: Molecular dynamics simulation and Multiwfn wave function analysis. *Colloids Surf. A Physicochem. Eng. Asp.* **2021**, *614*, 126186. [CrossRef]
131. Silva, D.T.C.; Fonseca, M.G.; Borrego-Sanchez, A.; Sainz-Díaz, C.I.; Soares-Sobrinho, J.L. Adsorption of tamoxifen on montmorillonite surface. *Microporous Mesoporous Mater.* **2020**, *297*, 110012. [CrossRef]
132. Shi, W.; Chu, Y.; Xia, M.; Wang, F.; Fu, C. The adsorption performance and micro-mechanism of MoS₂/montmorillonite composite to atenolol and acebutolol: Adsorption experiments and a novel visual study of interaction. *Ecotoxicol. Environ. Saf.* **2021**, *213*, 111993. [CrossRef] [PubMed]
133. Nguyen, H.C.; Fu, C.; Kao, D.; Tuong, T.; Tran, V.; Juang, R. Adsorption removal of tetracycline from water using poly (vinylidene fluoride)/polyaniline-montmorillonite mixed matrix membranes. *J. Taiwan Inst. Chem. Eng.* **2020**, *112*, 259–270. [CrossRef]
134. Malvar, L.J.; Martín, J.; Orta, M.; Medina-carrasco, S.; Luis, J.; Aparicio, I.; Alonso, E. Simultaneous and individual adsorption of ibuprofen metabolites by a modified montmorillonite. *Appl. Clay Sci.* **2020**, *189*, 105529. [CrossRef]
135. Peng, G.; Li, T.; Ai, B.; Yang, S.; Fu, J.; He, Q.; Yu, G.; Deng, S. Highly efficient removal of enrofloxacin by magnetic montmorillonite via adsorption and persulfate oxidation. *Chem. Eng. J.* **2019**, *360*, 1119–1127. [CrossRef]
136. Charaabi, S.; Tchara, P.-E.K.; Marminon, C.; Bouaziz, Z.; Holtzinger, G.; Pensé-Lhéritier, A.-M.; Le Borgne, M.; Issa, S. A comparative adsorption study of benzophenone-3 onto synthesized lipophilic organosilicate, Laponite and montmorillonite. *Appl. Clay Sci.* **2019**, *170*, 114–124. [CrossRef]
137. Okoyomon, O.O.; Kadir, H.A.; Zango, Z.U.; Saidu, U.; Nura, S.A. Physicochemical composition and heavy metal determination of selected industrial effluents of Ibadan. *Open J. Environ. Res.* **2021**, *2*, 58–66. [CrossRef]
138. Armaya, U.; Zango, Z.U.; Kadir, H.A.; Musawa, S.R. Assessment of Heavy Metals in Soils Samples from Lambun Sarki Irrigation Sites of Katsina Metropolis. *Resour. Environ.* **2020**, *10*, 4–9. [CrossRef]
139. Kumar Padhi, M.; Rath, D.; Nanda, B.B.; Kar, P.; Nanda, B. Solid waste derived montmorillonite clay as efficient photocatalytic system for removal of aquatic pollutants. *Environ. Nanotechnol. Monit. Manag.* **2022**, *17*, 100630. [CrossRef]
140. Anastopoulos, I.; Mittal, A.; Usman, M.; Mittal, J.; Yu, G.; Núñez-delgado, A.; Kornaros, M. A review on halloysite-based adsorbents to remove pollutants in water and wastewater. *J. Mol. Liq.* **2018**, *269*, 855–868. [CrossRef]
141. Chuaicham, C.; Xiong, Y.; Sekar, K.; Chen, W.; Zhang, L.; Ohtani, B.; Dabo, I.; Sasaki, K. A promising Zn-Ti layered double hydroxide/Fe-bearing montmorillonite composite as an efficient photocatalyst for Cr(VI) reduction: Insight into the role of Fe impurity in montmorillonite. *Appl. Surf. Sci.* **2021**, *546*, 148835. [CrossRef]
142. Ma, J.; Khan, M.A.; Xia, M.; Fu, C.; Zhu, S.; Chu, Y.; Lei, W.; Wang, F. Effective adsorption of heavy metal ions by sodium lignosulfonate reformed montmorillonite. *Int. J. Biol. Macromol.* **2019**, *138*, 188–197. [CrossRef] [PubMed]
143. Addy, M.; Losey, B.; Mohseni, R.; Zlotnikov, E.; Vasiliev, A. Adsorption of heavy metal ions on mesoporous silica-modified montmorillonite containing a grafted chelate ligand. *Appl. Clay Sci.* **2012**, *59–60*, 115–120. [CrossRef]
144. Vieira, R.M.; Vilela, P.B.; Becegato, V.A.; Paulino, A.T. Chitosan-based hydrogel and chitosan acid-activated montmorillonite composite hydrogel for the adsorption and removal of Pb⁺² and Ni⁺² ions accommodated in aqueous solutions. *J. Environ. Chem. Eng.* **2018**, *6*, 2713–2723. [CrossRef]
145. Ma, Q.; Ge, W.; Wu, C.; Xia, L.; Wang, W.; Song, S. MoS₂ composite hydrogel supported by two-dimensional montmorillonite nanosheets for Pb²⁺ removal from water. *Chem. Phys.* **2022**, *556*, 111477. [CrossRef]
146. De Pablo, L.; Chávez, M.L.; Abatal, M. Adsorption of heavy metals in acid to alkaline environments by montmorillonite and Ca-montmorillonite. *Chem. Eng. J.* **2011**, *171*, 1276–1286. [CrossRef]
147. Abdellaoui, Y.; Teresa, M.; Abatal, M.; Ali, B.; Emmanuel, S.; Díaz, M. Comparison of the divalent heavy metals (Pb, Cu and Cd) adsorption behavior by montmorillonite-KSF and their calcium- and sodium-forms. *Superlattices Microstruct.* **2019**, *127*, 165–175. [CrossRef]
148. Kalantari, K.; Ahmad, M.B.; Reza, H.; Masoumi, F.; Shamel, K.; Basri, M.; Khandanlou, R. Rapid and high capacity adsorption of heavy metals by Fe₃O₄/montmorillonite nanocomposite using response surface methodology: Preparation, characterization, optimization, equilibrium isotherms. *J. Taiwan Inst. Chem. Eng.* **2015**, *49*, 192–198. [CrossRef]
149. Zavala, M.Á.L.; Bouchez, B.F. Montmorillonite-perlite-iron ceramic membranes for the adsorption/removal of As (III) and other constituents from surface water. *Ceram. Int.* **2022**, *48*, 31695–31704. [CrossRef]
150. Abollino, O.; Aceto, M.; Malandrino, M.; Sarzanini, C.; Mentasti, E. Adsorption of heavy metals on Na-montmorillonite. Effect of pH and organic substances. *Water Res.* **2003**, *37*, 1619–1627. [CrossRef]
151. Khaldoun, A.; Wegdam, G.; Eiser, E.; Kerkeb, M.; Duran, J.G.; González-Caballero, F.; Bonn, D. Influence of heavy metals adsorption on the surface-energy properties of fluorinated montmorillonite clays “Rassoul”. *Colloids Surf. A* **2006**, *290*, 1–6. [CrossRef]

152. Yang, S.; Cheng, Y.; Wang, Y.; Liu, L.; Li, Y.; Wang, D.; Qian, J. Construction Si-O-Mo bond via etching method: Enhancing selective adsorption capacity of MoS₂/montmorillonite to Pb²⁺. *Mater. Today Chem.* **2022**, *26*, 101056. [[CrossRef](#)]
153. Jiang, K.; Liu, K.; Peng, Q.; Zhou, M. Adsorption of Pb (II) and Zn (II) ions on humus-like substances modified montmorillonite. *Colloids Surf. A Physicochem. Eng. Asp.* **2021**, *631*, 127706. [[CrossRef](#)]
154. Kameda, T.; Honda, R.; Kumagai, S.; Saito, Y.; Yoshioka, T. Adsorption of Cu²⁺ and Ni²⁺ by tripolyphosphate-crosslinked chitosan-modified montmorillonite. *J. Solid State Chem.* **2019**, *277*, 143–148. [[CrossRef](#)]
155. Ordinartsev, D.; Pechishcheva, N.; Estemirova, S.; Kim, A.; Shunyaev, K. Removal of Cr (VI) from wastewater by modified montmorillonite in combination with zero-valent iron. *Hydrometallurgy* **2022**, *208*, 105813. [[CrossRef](#)]
156. Miao, Y.; Peng, W.; Wang, W.; Cao, Y.; Li, H.; Chang, L. 3D-printed montmorillonite nanosheets based hydrogel with biocompatible polymers as excellent adsorbent for Pb (II) removal. *Sep. Purif. Technol.* **2022**, *283*, 120176. [[CrossRef](#)]
157. Nguyen, T.T.; Hoang, B.N.; Van Tran, T.; Nguyen, T.D.; Vo, D.V.N. Agar/maltodextrin/poly (vinyl alcohol) walled montmorillonite composites for removal of methylene blue from aqueous solutions. *Surf. Interfaces* **2021**, *26*, 101410. [[CrossRef](#)]
158. Li, P.; Huang, L.; Li, Y.; Xu, Y.; Huang, S.; Yuan, D.; Xu, H.; Li, H. Synthesis of dark orange montmorillonite/g-C₃N₄ composites and their applications in the environment. *J. Phys. Chem. Solids* **2017**, *107*, 131–139. [[CrossRef](#)]
159. Shang, Q.; Liu, X.; Zhang, M.; Zhang, P.; Ling, Y.; Cui, G.; Liu, W.; Shi, X.; Yue, J.; Tang, B. Photocatalytic degradation of ofloxacin antibiotic wastewater using TS-1/C₃N₄ composite photocatalyst: Reaction performance optimisation and estimation of wastewater component synergistic effect by artificial neural network and genetic algorithm. *Chem. Eng. J.* **2022**, *443*, 136354. [[CrossRef](#)]
160. Huang, Z.; Wu, P.; Gong, B.; Yang, S.; Li, H.; Zhu, Z.; Cui, L. Preservation of glutamic acid-iron chelate into montmorillonite to efficiently degrade Reactive Blue 19 in a Fenton system under sunlight irradiation at neutral pH. *Appl. Surf. Sci.* **2016**, *370*, 209–217. [[CrossRef](#)]
161. Baizig, M.; Khalfallah, S.; Bassem, J.; Batis, N.; Trujillano, R. Preparation and Characterization of Different TiO₂-Modified Montmorillonite Meso-Microporous Materials, with Enhanced Photocatalytic Activity. *Int. J. Eng. Res. Technol.* **2015**, *4*, 182–192.
162. Abderrahim, N.; Djellabi, R.; Ben Amor, H.; Fellah, I.; Giordana, A.; Cerrato, G.; Di Michele, A.; Bianchi, C.L. Sustainable purification of phosphoric acid contaminated with Cr(VI) by Ag/Ag₃PO₄ coated activated carbon/montmorillonite under UV and solar light: Materials design and photocatalytic mechanism. *J. Environ. Chem. Eng.* **2022**, *10*, 107870. [[CrossRef](#)]